Prediction of thermodynamic properties of refrigerant fluids with a new three-parameter cubic equation of state

Christophe Coquelet, Céline Houriez, Jamal El Abbadi

Prediction of thermodynamic properties of refrigerant fluids with a new three-parameter cubic equation of state

Prédiction des propriétés thermodynamiques des fluides frigorigènes avec une nouvelle équation d'état cubique à trois paramètres

Christophe Coquelet[1]**, Jamal El Abbadi, Céline Houriez**

Mines ParisTech, PSL Research University, CTP – Centre Thermodynamique des Procédés, 35 rue Saint Honoré, 77305 Fontainebleau Cedex, France

Abstract

To describe the thermodynamic properties of refrigerant fluids, it is important to use a reliable thermodynamic model able to predict accurate results for both pure compounds and mixtures. In this study, a new three-parameter cubic equation of state is presented, based on the modification of the well-known Patel-Teja equation of state. The new equation of state is associated with the Mathias-Copeman alpha function.
By only knowing the acentric factor ω and the experimental critical compressibility factor Z_c of pure compounds, it is possible to predict thermodynamic properties for both pure compounds and mixtures by means of the new equation of state. No binary interaction parameter k_{ij} is needed for the prediction of mixture properties.
The results obtained with the new equation of state show a good agreement with experimental data for vapor-liquid equilibrium and density properties. The obtained results are particularly satisfying for liquid density, and in the vicinity of the critical point, by comparison with the results obtained using the Peng-Robinson and the Patel-Teja equations of state.

Keywords: Equation of state, density, vapor-liquid equilibrium, refrigerant fluids, fluorinated compounds

Mots clés: Equation d'état, densités, équilibre liquide-vapeur, fluides réfrigérants, composés fluorés

[1] Corresponding author. Email address: christophe.coquelet@mines-paristech.fr; Tel.: +33164694962 / +33164694963; Fax: +33164694968

Symbols and abbreviations

a	Cohesive energy parameter (J m^3 mol^{-2})
ARD	Average relative deviation
b	Covolume parameter (m^3 mol^{-1})
EoS	Equation of state
CEoS	Cubic equation of state
F_{obj}	Objective function
k_{ij}	Binary interaction parameter
m_n	Alpha function parameter
NEoS	Our new equation of state
MC	Mathias-Copeman
P	Pressure (MPa) / 1MPa = 10^6 Pa
PR	Peng-Robinson
PT	Patel-Teja
SRK	Soave-Redlich-Kwong
R	Gas constant (J mol^{-1} K^{-1})
T	Temperature (K)
v	Molar volume (m^3 mol^{-1})
x	Liquid mole fraction
y	Vapor mole fraction
Z	Compressibility factor
HFCs	Hydrofluorocarbons
HFOs	Hydrofluoroolefins
HCFO	Hydrochlorofluoroolefins
GWP	Global warming potential

Greek letters

ω	Acentric factor
α	Alpha function
Ω_a, Ω_b, Ω_c	Substance depending factors
ρ	Molar density (mol m^{-3})

Subscripts

c	Critical property
cal	Calculated property

exp	Experimental property
i,j	Molecular species
opt	Optimized property
r	Reduced property

Superscripts

V	Vapor phase
L	Liquid phase

1. Introduction

For several years, new-generation refrigerants are proposed, in order to reduce the overall emission of greenhouse gases (Kyoto protocol, 1997) and to respect the environmental regulations issued by the European Union (F-gas regulations) [1]. In particular, due to their low global warming potential (GWP), hydrofluoroolefins (HFOs), such as the R-1234yf (2,3,3,3-tetrafluoropropene) and the R-1234ze (trans-1,3,3,3-tetrafluoropropene), arouse interest and have been proposed as replacements for some previous-generation fluids such as the 1,1,1,2-tetrafluoroethane (R-134a) [2]. However, the use of pure component fluid may not be suitable for some refrigeration applications, due to performance and safety concerns. Thus, blends of refrigerants are often considered, including for instance a HFO, a hydrofluorocarbon (HFC), and CO_2, such as the R-445A blend.
The detailed knowledge of the thermodynamic properties of refrigerants, and particularly of their vapor-liquid equilibrium (VLE) behavior, is essential to design and optimize thermodynamic systems involving refrigerants, from the production and separation units to the refrigerant-based systems (such as air-conditioning systems, organic Rankine cycles, heat pumps etc.). In the field of refrigeration, there is a strong need for thermodynamic data of fluids, either to retrofit existing equipments with alternative refrigerants or to replace these equipments. In particular, when developing an alternative refrigerant, the list of possible mixtures is very large, and to obtain detailed experimental data for all the promising candidates can become rapidly time-consuming and expensive.
As a complement to experiment, equations of state (EOSs) are one of the most convenient tools to correlate, extrapolate and predict thermodynamic properties and phase behavior for pure fluids and mixtures. For instance, they can be very useful to screen possible fluid candidates for their suitability in a particular application. Since van der Waals introduced his famous EoS in 1873 [3], cubic EoSs (CEoSs) have been subject to active research and improvements, and were widely used in industrial process design and optimization, due to their accuracy, generality, simplicity and speed of computation [4], [5].
The Soave-Redlich-Kwong (SRK) and Peng-Robinson (PR) equations are among the most popular cubic EoSs and are used for many applications, in which thermodynamic and VLE properties are required.
Concerning the vapor pressures, the capacity of prediction of the cubic EoSs is related to the model chosen for the temperature-dependent alpha function, while the prediction of volumetric properties depends on the volume function [5]–[8]. For instance, in the PR-EoS,

the modification of the volume dependency of attractive term represents an improvement upon SRK-EoS, and allows one to obtain better results for liquid densities and better representation of VLE for many mixtures [5], [6], [9].
One of the drawbacks of the two-parameter cubic EoSs is that they involve a critical compressibility factor Z_c whose value is constant, regardless of the substance, providing saturated liquid densities and critical densities different from the experimental ones [7], [10].
A popular approach to improve molar volumes (and by consequence densities) is the volume translation method, introduced by Péneloux et al. [11]. Details concerning application of a Péneloux-type volume translation to an EoS can be find in a recent paper by Jaubert et al. [12] who discussed the effects of using such a volume translation on the different calculated thermodynamic properties,.
Another approach consists in developing van der Waals-type EoSs with three or more parameters, properly adjusted to correlate simultaneously the saturated densities and the vapor pressure of pure components [13].
In this work, we follow this latter approach, by using a substance-dependent critical parameter instead of a fixed value of Z_c [14], to improve saturated liquid densities and critical densities. By doing so, we obtain a three-parameter equation of state. Note that it has been shown that the optimal value of the critical compressibility factor is generally different from the experimental one [14], [15].
One of the well-known three-parameter equation of state is the Patel-Teja (PT) EoS and its generalized form [16], [17], which has been successfully applied to correlate mixture VLE data [18].
The three-parameter cubic EoS proposed in this work (denoted by NEoS), which is a modification of the PT-EoS, is based on the use of an optimized substance-dependent critical compressibility factor, yielding better representation of liquid densities. The NEoS is associated with the Mathias-Copeman alpha function.
By applying the NEoS to pure compound refrigerants, we were able to develop correlations relating the alpha function parameters to the acentric factor, and the optimized critical compressibility factor to the experimental one. As a result, the NEoS can be used for a wide range of refrigerants for which no experimental data are available. Furthermore, in this work, we show that by only calculating for pure compounds the alpha function parameters and the optimized critical compressibility factor, from the correlations developed, we can extend the prediction to mixtures. This has been done without need of VLE experimental data, and with no adjustment of the binary interaction parameter k_{ij} (as we worked with $k_{ij} = 0$).
In this study, we present the results of prediction obtained with the NEoS for the pure compounds R-1234yf, R-1216 (hexafluoropropylene), CO_2, and R-134a, for the binary mixtures R-421A (pentafluoroethane R-125 + R-134a), and R-508A (trifluoromethane R-23 + hexafluoroethane R-116), and for the ternary mixture R-404A (R-125 + 1,1,1-trifluoroethane R-143a + R-134a). The NEoS results are compared to those obtained using the PT and the PR EoSs.

2. Model

2.1. Description of the NEoS

In order to predict accurately the thermodynamic properties of refrigerants (both pure compounds and mixtures), a new EoS (denoted by NEoS) was developed, based on the modification of the well-known PT-EoS [16].
The NEoS is a three-parameter cubic EoS and is defined by the following relation:

$$P = \frac{RT}{v-b} - \frac{a(T)}{v^2 + ubv + wb^2} \quad (1)$$

where P is the pressure, T the temperature, v the volume, and R the universal constant for ideal gases. b is the volumetric parameter and a(T) the cohesive energy parameter.
u and w are two parameters defined in order to have: u + w = 0, which was shown to be the optimal combination for liquid density calculations by cubic EoSs [10] - other authors such as Segura et al. [13] work on similar approaches, by the parameterization of u and w, without fixing a relation between them.
Here, u and w are defined as follows:

$$u = 1 + \frac{c}{b}$$
$$w = -u \quad (2)$$

While the PT-EoS [10], [16], [19] and the NEoS have the same definition for u, a different definition for w is chosen in the NEoS in order to fulfil the conditions defined by Ji and Lempe [10], i.e. u + w = 0 (note that in the case of the PT-EoS, u + w = 1).
The cohesive energy parameter a(T) depends on the temperature and is defined as follows:

$$a(T) = a_c \alpha(T) \quad (3)$$

α(T) is the alpha function that will be defined below, and which depends on both the temperature and the substance.
The parameters a_c, b and c of Eq. (1)-(3) can conventionally be obtained from the thermodynamic conditions at the critical point, defined as follows:

$$\left(\frac{\partial P}{\partial v}\right)_{T_c} = \left(\frac{\partial^2 P}{\partial^2 v}\right)_{T_c} = 0 \quad (4)$$

Or from the mathematical constraint:

$$(v - v_c)^3 = v^3 - 3v_c v^2 + 3{v_c}^2 v - {v_c}^3 = 0 \quad (5)$$

where v_c is the optimized critical volume.

After rewriting Eq. (1), we obtain:

$$v^3 - \left[\frac{RT}{P} - (u-1)b\right]v^2 + \left[\frac{RT}{P}ub - (w-u)b^2 - \frac{a}{P}\right]v - \frac{RT}{P}wb^2 + wb^3 + \frac{ab}{P} = 0 \quad (6)$$

The parameters a_c, b and c are calculated according to the relations:

$$a_c = \Omega_a \frac{R^2 {T_c}^2}{P_c}$$

$$b = \Omega_b \frac{RT_c}{P_c} \tag{7}$$

$$c = \Omega_c \frac{RT_c}{P_c}$$

where Ω_a, Ω_b and Ω_c are factors depending on the substance [19], T_c and P_c are respectively the experimental critical temperature and pressure.

We set $T = T_c$ and $P = P_c$ in Eq. (6), then the comparison with Eq. (5) results in:

$$\Omega_a = 1 - 3Z_{C,opt}\left(1 - Z_{c,opt}\right) + 3(1 - 2Z_{c,opt})\Omega_b + [2 - (u + w)]{\Omega_b}^2$$

$${\Omega_b}^3 + \left[\left(1 - 3Z_{c,opt}\right) + (u + w)\right]{\Omega_b}^2 + 3Z_{c,opt}^2\,\Omega_b - Z_{c,opt}^3 = 0 \tag{8}$$

$$\Omega_c = 1 - 3Z_{c,opt}$$

$Z_{c,opt}$ is an apparent optimized critical compressibility factor. It is different from the experimental critical compressibility factor Z_c, and adjusted from the experimental VLE data [10], [20], in order to improve the prediction of liquid densities.
Here, as u + w = 0, we can simplify Eq. (6) to obtain:

$$\Omega_a = 1 - 3Z_{C,opt}\left(1 - Z_{c,opt}\right) + 3(1 - 2Z_{c,opt})\Omega_b + 2{\Omega_b}^2$$

$${\Omega_b}^3 + (1 - 3Z_{c,opt})\,{\Omega_b}^2 + 3Z_{c,opt}^2\,\Omega_b - Z_{c,opt}^3 = 0 \tag{9}$$

By including the critical compressibility factor in the calculations, better results can be obtained, even though the apparent critical compressibility factor $Z_{c,opt}$ is larger than the experimental one, Z_c.

2.2. Mathias-Copeman alpha function

The NEoS is associated with the Mathias-Copeman (MC) alpha function [21], which is defined as follows:

$$\alpha(T) = \left[1 + m_1\left(1 - \sqrt{\frac{T}{T_c}}\right) + m_2\left(1 - \sqrt{\frac{T}{T_c}}\right)^2 + m_3\left(1 - \sqrt{\frac{T}{T_c}}\right)^3\right]^2 ; \quad if\ T < T_c$$

$$\alpha(T) = \left[1 + \mathrm{m}_1\left(1 - \sqrt{\frac{T}{T_c}}\right)\right]^2 ; \quad if\ T > T_c \tag{10}$$

2.3. Parameters adjustment

To manage and treat the experimental data, we used an in-house software, allowing the adjustment and the calculations of the thermodynamic properties for pure components.
In order to predict the thermodynamic properties for different fluids, the parameters of the alpha function, m_1, m_2, and m_3, and the optimized critical compressibility factor $Z_{c,opt}$ were adjusted from data of 34 pure compounds obtained by using REFPROP 9.0 [22].
For the calculations, we used a modified simplex algorithm. The objective function (in the case of NEoS and PT-EoS) contains vapor pressures and liquid densities and is defined as follows:

$$F_{obj} = \frac{100}{N}\left[\sum_1^N\left(\frac{P_{exp} - P_{cal}}{P_{exp}}\right)^2 + \sum_1^N\left(\frac{\rho_{exp}^L - \rho_{cal}^L}{\rho_{exp}^L}\right)^2\right] \tag{11}$$

In the case of the PR-EoS, the objective function contains vapor pressures and is as follows:

$$F_{obj} = \frac{100}{N}\left[\sum_1^N\left(\frac{P_{exp} - P_{cal}}{P_{exp}}\right)^2\right] \tag{12}$$

N is the number of data points, P_{exp} is the experimental vapor pressure, P_{cal} the calculated vapor pressure, ρ^L_{exp} the experimental saturated liquid density and ρ^L_{cal} the calculated saturated liquid density.

To estimate the parameters, we need the values of the critical pressure P_c, the critical temperature T_c, the experimental critical compressibility factor Z_c (in the case of PR-EoS, Z_c is fixed at 0.3074), and the acentric factor ω. We need also the data of the vapor pressures P^{sat}, as well as the saturated liquid densities ρ^L for different temperatures (for the NEoS and PT-EoS; for PR-EoS, only the data of vapor pressures are required).
In this work, the temperatures range from the triple point temperature to the critical temperature (T_c), with a step of 1 K.

For the NEoS, PT-EoS, and PR-EoS, we estimate the alpha function parameter m_1, while the parameters m_2 and m_3 were set to constant values. For the NEoS and PT-EoS, the optimized critical compressibility factor $Z_{c,opt}$ is also estimated, while the Z_c value is 0.3074 for the PR-EoS.

For the three CEoSs, we carried out the parameter determination by associating each EoS with the MC alpha function, leading to three different sets of parameters. Here, only the estimated parameters for the NEoS with the MC alpha function are presented (Cf. Table 1) and the parameters for both PT-EoS and PR-EoS are provided in Appendices A and B, respectively.

Based on these adjusted parameters, we established a correlation between the alpha function parameter m_1 and the acentric factor ω, as well as a correlation between the optimized critical compressibility factor $Z_{c,opt}$ and the experimental one Z_c.
In this way, we can calculate the alpha parameters and the optimized critical compressibility factor for other compounds, whose thermodynamic properties are not known experimentally, allowing us to predict their thermodynamic properties.
The correlations obtained with the NEoS are shown in Fig. 1 and given in Eq. (11).

From the graphical representations, we can see a correlation between the alpha function parameter m_1 and the acentric factor ω, and between the optimized critical compressibility factor $Z_{c,opt}$ and the experimental one Z_c. Based on our calculations, the parameters m_2 and m_3 are taken as constants.

$$\begin{aligned} m_1 &= 2.7868\omega^2 - 0.2376\omega + 0.3007 \\ m_2 &= 0.47 \\ m_3 &= -0.08 \\ Z_{c,opt} &= -7.4737 Z_c^{\,2} + 4.8824 Z_c - 0.4900 \end{aligned} \tag{13}$$

The same work has been carried out for the other EoSs considered here, PT-EoS and PR-EoS, and the correlations developed for these EoSs are provided in Appendices A and B, respectively.

3. Results and discussions

3.1. Pure compounds

Based on the correlations developed, and using the parameters calculated from it, we predicted the thermodynamic properties of four pure compound refrigerant fluids: R-1234yf, R-1216, CO_2 and R-134a.
The results of the prediction were compared to the results obtained from REFPROP 9.0. The P-ρ diagram has been predicted at saturation and out of saturation.

3.1.1. R-1234yf: Prediction at saturation

The prediction at saturation was performed using the three EoSs, and were compared to the results from REFPROP 9.0, as well as to experimental data [23], [24]. The results were calculated from the triple point temperature to the critical temperature.
The parameters of the MC alpha functions and the critical compressibility factors were calculated from the correlations given in Eq. (11) (for the PR-EoS, the value of Z_c is set to 0.30740). The values obtained for these parameters are reported in Table 2.

The graphical representation of the P-ρ diagram at saturation is shown in Fig. 2.

Based on the results of the prediction, we calculated the average relative deviation (ARD), the BIAS, and the relative deviation (RD) for each EoS considered here, compared to the results obtained from REFPROP 9.0. The ARD, the BIAS and the RD are defined by Eq. (14):

$$ARD(X)\ \% = \left| \frac{100}{N} \sum_{1}^{N} \frac{X_{exp} - X_{cal}}{X_{exp}} \right|$$

$$BIAS\ (X)\ \% = \frac{100}{N} \sum_{1}^{N} \frac{X_{exp} - X_{cal}}{X_{exp}} \qquad (14)$$

$$RD\ X\ (\%) = 100 * \frac{X_{exp} - X_{cal}}{X_{exp}}$$

The ARD and the BIAS calculated using the parameters of the correlations are reported in Table 4.a, while the ARD and the BIAS calculated using the adjusted parameters are in Table 3.

From the results of the prediction represented in Fig. 2, we can see that the NEoS provides a better representation for the liquid density compared to PR-EoS and PT-EoS, especially at high temperature and in the vicinity of the critical point. We can also see that with the NEoS, it is possible to reproduce more accurately the location of the critical point, compared to the other two EoSs [ρ_c(NEoS) = 3961 mol m^{-3}; ρ_c(PT-EoS) = 3573 mol m^{-3}; ρ_c(PR-EoS) = 3597 mol m^{-3}; ρ_c(REFPROP) = 4170 mol m^{-3}].
The vapor pressure and the vapor density appear to be well represented by the three EoSs, with the better results obtained with the PR-EoS for vapor density.
From Table 3, we can notice that by using the adjusted parameters instead of the parameters calculated from the correlations, the results are improved for the ARD and the BIAS.

Based on the results obtained, we represented the RD as a function of the temperature, using the NEoS (Cf. Fig. 3).

From the RD representation, we can see that the vapor pressure is overestimated at low temperature, and that the RD tends to 0 with increasing temperature.
The vapor density is overestimated at low and high temperatures and well represented at intermediate temperatures.
The liquid density is underestimated at low and high temperatures, and well represented at intermediate temperatures.

3.1.2. R-1234yf: Prediction out of saturation

For the prediction out of saturation (section 3.1.1), we used the same three EoSs as for the prediction at saturation. Four isotherms are considered here, for a reduced temperature T_r of 0.7, 0.9, 1, and 1.1. Note that the critical temperature of R-1234yf is 367.85 K [22].
The graphical representation of the P-ρ diagram for the four isotherms out of saturation is shown in Fig. 2.

From Fig. 2, we can see that the NEoS leads to better results for the liquid density than the PT-EoS and PR-EoS. Furthermore, with the NEoS it is possible to represent rather accurately the density at supercritical conditions, while the PT-EoS and PR-EoS show important deviations in this region, compared to the REFPROP results. Concerning the vapor density, it appears to be well represented by the three EoSs considered.

3.1.3. R-1216, CO_2, and R-134a: Prediction at saturation

The same study was carried out for the hexafluoropropylene (R-1216), the carbone dioxide (CO_2), and the 1,1,1,2-tetrafluoroethane (R-134a), using the three CEoSs. The results were predicted from the triple point temperature to the critical temperature (for R-1216, the results are for T_r from 0.6 to 1).
The critical temperature of R-1216, CO_2, and R-134a are respectively 358.9 K [25], 304.13 K [22], and 374.21 K [22].
The parameters of the MC alpha functions and the critical compressibility factor were calculated from the correlations established. The values of these parameters are reported in Table 2.

The graphical representations of the P-ρ diagram at saturation, using the three CEoSs associated with the MC alpha function, are shown in Fig. 4, 5, and 6. The results are compared to REFPROP and experimental data [25], [26].

The ARD and the BIAS were calculated for the results obtained with the EoSs, compared to the results of REFPROP 9.0 (experimental results in the case of R-1216). The values obtained for the ARD and the BIAS are reported in Table 4.a.

From Fig. 4 to 6 and Table 4.a, the same conclusions as for R-1234yf can be drawn in the case of R-1216, CO_2, and R-134a. For these three compounds, the NEoS provides a better representation of the saturated liquid density in general, and especially in the critical region. The PT-EoS and PR-EoS show deviations, relative to experiment and REFPROP, in representing the saturated liquid density, particularly in the case of the R-1216.
The saturated vapor density and the vapor pressure are well represented by all the three EoSs, with better results when using PR-EoS.

3.1.4. R-1216, CO_2, and R-134a: Prediction out of saturation

As for R-1234yf, the prediction out of saturation for R-1216, CO_2, and R-134a was performed for four isotherms, with T_r = 0.73, 0.9, 1, and 1.01 in the case of R-1216, T_r = 0.8, 0.9, 1, and 1.1 in the case of CO_2, and T_r = 0.7, 0.9, 1, and 1.1 in the case of R-134a.
The graphical representation of the P-ρ diagram for the four isotherms studied out of saturation is shown in Fig. 4, 5, and 6.

From the Fig. 4 to 6, the NEoS provides a better representation of the liquid density than the PT-EoS and PR-EoS. In addition, with the NEoS it is possible to represent accurately the density at supercritical conditions.
In the case of the R-1216, we can see that the PT-EoS and PR-EoS lead to important deviations in the prediction of the liquid density, relative to the experimental data, while the NEoS results are close to experiment.
For the CO_2 and R-134a, the representation of the liquid density at T_r = 0.9 obtained by using the NEoS is not in very good agreement with the REFPROP results, however, the PT-EoS and PR-EoS fail also to reproduce these results.
The vapor phase is in overall well represented by the three EoSs for all the isotherms considered.

3.2. Mixtures

For the mixtures, the classical van der Waals mixing and combining rules [27] have been used for the calculations:

$$a = \sum_{i=1}^{N}\sum_{j=1}^{N} x_i x_j a_{ij}$$

$$a_{ij} = \left(1 - k_{ij}\right)\sqrt{a_i a_j} \quad , \quad i = 1,2 \ldots . N \quad , \quad j = 1,2 \ldots . N \tag{15}$$

$$b = \sum_{i=1}^{N} x_i b_i$$

$$c = \sum_{i=1}^{N} x_i c_i$$

where x_i is the mole fraction of the component i, a_i is the energy parameter, and b_i and c_i are the covolume parameters of the component i, and k_{ij} is the binary interaction parameter. N is the number of components of the system.

3.2.1. VLE (Vapor-liquid equilibrium) calculation

The VLE calculation was performed for 12 different binary mixtures of refrigerants by using the NEoS, and the obtained results were compared to experiment. The experimental data used were collected from the literature [28]–[38]. The results of the calculation are shown in Fig. 7 to 18.

For some systems, the binary interaction parameter k_{ij} was set to 0, and we obtained accurate results compared to the experimental ones (Fig. 9 to 12). For the systems more delicate to model, like the azeotropic ones, we noticed that with k_{ij} set to 0, it is not possible to represent the azeotropic behavior. An adjusted k_{ij} parameter is thus needed in this case (Fig. 13 to 18). We can also note that for supercritical temperatures, an adjusted k_{ij} parameter leads to more accurate results than a k_{ij} set to 0.

In addition, the ARD and the BIAS of the pressure and the vapor composition were calculated for the binary mixtures studied in this section. The ARD and the BIAS were calculated comparing to the experimental data collected from the literature. The results are reported in Table 4.b.

The k_{ij} values were adjusted for each isotherm by using the NEoS. For the sake of comparison, we give also the values of k_{ij} fitted by using the PR-EoS. The k_{ij} values used for the azeotropic and supercritical systems studied are reported in Table C.1 (Table C.1 is provided as supplementary content).

From the Table C.1, we can note that lower k_{ij} values are generally obtained when using the NEoS compared to the PR-EoS. These k_{ij} values are represented as a function of temperature in Fig. C.1 to C.6, for the six systems for which an adjusted k_{ij} value was used (Fig. C.1 to C.6 are provided as supplementary content). From these latter figures, we can note a correlation between k_{ij} and the temperature, with the NEoS and PR-EoS, for the different binary systems

considered here. For the systems whose one component has its critical temperature in the range considered (Fig. C.1 and C.2), we can see a discontinuity of the $k_{ij}(T)$ function: two correlations have thus been employed for these latter systems, depending on if we are below or above the critical temperature. For the CO_2 + R-32 system (Fig. C.1), we note that the correlation between k_{ij} and the temperature is not very strong above the critical temperature of CO_2 with NEoS, while it is better with the PR-EoS (coefficients of determination respectively equal to 0.58 and 0.99).

For the SO_2 + R-32 system (Fig. C.2), in the case of the NEoS, there is a strong correlation between k_{ij} and the temperature, both below and above the critical temperature of CO_2 (both coefficients of determination around 0.96), while with the PR-EoS, the correlation is weaker (coefficients of determination equal to 0.51 and 0.78, respectively below and above the critical temperature).

From Fig. 13 to 18, we can clearly see that considering an adjusted binary interaction parameter k_{ij} is necessary to model accurately the VLE behavior of some systems. Indeed, a k_{ij} parameter is needed for systems including asymmetric components (in terms of molecular size, and nature and strength of intermolecular interactions, such as the quadrupolar ones, for instance).

It would be interesting to assess the effect of using mixing rules more complex than the van der Waals ones, such as g^E –mixing rules, and of adding a polar term to the NEoS, to take into account the polarity of refrigerants.

Inspired from the work of Jaubert and coworkers [39]–[43], an additional path that could be interesting to investigate is to apply a group contribution method to the NEoS, allowing the use of the van der Waals mixing rules, and to calculate a predictive k_{ij}.

3.2.2. Binary mixtures: R-421A and R-508A

Based on the correlations and the parameters calculated for the pure compounds, we studied the two binary systems:
- R-421A, which is a mixture at fixed composition of R-125 (58 wt%) and R-134a (42 wt%);
- R-508A which is a mixture at fixed composition of R-23 (39 wt%) and R-116 (61 wt%).
The prediction was performed using the three above-mentioned EoSs, associated with the MC alpha function. The MC alpha function parameters and the critical compressibility factor were calculated from the correlations established in section 2.3 and their values are reported in Table 2.

The predicted pressure-density diagrams are shown in Fig. 19 and 20, together with the results obtained from REFPROP 9.0. The prediction out of saturation was performed for four isotherms: T_r = 0.7, 0.9, 1.0, 1.1. The critical temperatures are 355.93 K for R-421A and 283.34 K for R-508A [22].

From Fig. 19 and 20, we can see that the NEoS provides a better representation for the liquid density, both at saturation and out of saturation, especially at low (T_r = 0.7) and critical temperatures, for the two systems R-421A and R-508A. Note that the PR-EoS and PT-EoS fail to represent accurately the liquid densities of the two systems considered here at saturation, and at T_r = 0.7 and T_r = 1.0, while the vapor densities out of saturation appear to be well represented by the three EoSs.
However, for the vapor density at saturation, we can see from Table 4.a that the deviations to the REFPROP results are quite large for the R-421A. For the R-508A, the deviations are smaller, and we obtain the best results with the NEoS, compared to the PR-EoS and PT-EoS.
For the R-421A, for T_r = 1.0, the results predicted by the three EoSs don't match very well the REFPROP results when increasing pressure, however, the best agreement is obtained with the NEoS, relative to PR-EoS and PT-EoS. For the R-508A, for T_r = 0.9, the PR-EoS and PT-EoS provide results in slightly better agreement with the REFPROP results, compared to the NEoS.

3.2.3. Ternary mixture: R-404A

In this section, we study the ternary system R-404A, which is a mixture of R-125 (44 wt%), R-134a (4 wt%), and R-143a (52 wt%). The same work as described in section 3.2.2 for the binary mixtures was carried out for the R-404A system.
The prediction was performed using the three EoSs presented above, associated with the MC alpha function. The MC alpha function parameters and the critical compressibility factor were calculated with the correlations established (Cf. Table 2).

The results of the prediction for the pressure-density diagram were compared to the results obtained from REFPROP 9.0. (Cf. Fig. 27). The prediction out of saturation was performed for four isotherms: T_r = 0.7, 0.9, 1.0, 1.1. The critical temperature of the R-404A is estimated to be T_c = 345.2 K [22].

For the ternary mixture R-404A, and as we can see from Fig. 27, the NEoS gives a good representation of the density at the critical and supercritical temperatures, compared to the PT-EoS and PR-EoS, but the NEoS results are less satisfactory at subcritical temperatures for

liquid density. However, the saturation liquid density is well represented by using the NEoS, relative to the other two EoSs.
For T_r = 0.7, the PT-EoS provides results in better agreement with REFPROP results, compared to the PR-EoS and NEoS.
For T_r = 0.9, the three EoSs fail to represent accurately the liquid density. The vapor density appears to be well represented by the three EoSs for all the isotherms considered.
However, for the vapor density at saturation, and as we can see from Table 4.a, the deviations to REFPROP are quite large with the three EoSs.

4. Conclusion

In this paper, we introduced a new three-parameter cubic equation of state based on the principle of corresponding states.
This EoS was used for the study of refrigerant fluids including pure component, binary, and ternary fluids: R-1234yf, R-1216, CO_2, R-134a, R-421A, R-508A, and R-404A. The NEoS was used to predict the thermodynamic properties of these fluids, such as the pressure-x-y and pressure-density diagrams, and the results obtained were compared to the PT-EoS and PR-EoS ones.

The three EoSs considered in this paper were associated with the MC alpha function. The parameters of this alpha function, as well as the optimized critical compressibility factor (for the NEoS and the PT-EoS), were calculated based on the correlations established in the present work.
For the binary and ternary systems, the binary interaction parameters k_{ij} was set to 0, without any fitting to experimental data. However, for some systems, such as the azeotropic ones, it has been necessary to consider a k_{ij} parameter to accurately represent the VLE behavior of the systems. Indeed, for instance, the refrigerant compounds are characterized by a large heterogeneity in terms of molecular properties, as some compounds possess strong dipole and/or quadrupole moments and other compounds only weak multipole moments. This may be why a k_{ij} parameter is needed to model some of the binary systems considered.
It would also be interesting to test other mixing rules than the van der Waals ones, such as g^E –mixing rules, or to add a polar term in the NEoS to take into account the polarity of some refrigerant compounds.
An additional path that could be interesting to investigate is the combination of the NEoS with a group contribution method to calculate the k_{ij} of van der Waals mixing rules, as it is done successfully with the PPR78 model [39]–[43].

Together, the results of the predictions for the pure compounds and for the binary and ternary mixtures show that the NEoS provides a better representation of the liquid density at saturation and out of saturation, compared to the results obtained with the PT-EoS and PR-EoS. The results are also better for the density in the critical region. However, the NEoS prediction concerning the ternary mixture could be improved for the subcritical temperatures.
The density in the critical region is well represented by using the NEoS, compared to the other EoSs considered in this work. However, this prediction could be better by combining the NEoS with a renormalization group theory [44], [45], using a crossover approach [46], [47] or the White's recursive method [48]. Such a study will be carried out in a future work.

In overall, the NEoS provides a better representation of the densities, which are essential for the prediction of transport properties (viscosity, thermal conductivity…), and it would be particularly interesting to couple the NEoS with the TRAPP method [49], [50], for instance.
The prediction ability of VLE (without k_{ij}) for complex systems with the NEoS is limited, however, from the results presented in this paper concerning refrigerants, the NEoS shows better density prediction potentialities (without k_{ij}) than the PR-EoS and PT-EoS, and this EoS deserves thus to be tested in process simulators for industrial purpose.

Appendices

A. Patel-Teja EoS

In Table A-1 are reported the alpha function parameters and the critical compressibility factor adjusted from vapor pressure and saturated liquid density of pure compounds, obtained using PT-EoS associated with the MC alpha function.

Based on this adjustment, correlations were established, relating the alpha function parameters to the acentric factor ω, and the optimized critical compressibility factor to the experimental one. The results are reported in Eq. (A.1).

$$\begin{gathered} m_1 = 3.6410\omega^2 - 0.5673\omega + 0.6142 \\ m_2 = -0.01 \\ m_3 = 0.4 \\ \mathrm{Z_{c,opt}} = -11.356\mathrm{Z_c}^2 + 6.8984\mathrm{Z_c} - 0.7266 \end{gathered} \tag{A.1}$$

In Fig. A.1 are shown the correlations relating the alpha function parameter m_1 to the acentric factor ω, and the optimized critical compressibility factor to the experimental one.

B. Peng-Robinson EoS

In Table B-1 are reported the alpha function parameters adjusted from vapor pressure of pure compounds, obtained using PR-EoS associated with the MC alpha function.

Based on this adjustment, a correlation was established, relating the alpha function parameters to the acentric factor ω. The results are reported in Eq. (B.1).

$$\begin{gathered} m_1 = -0.0944\omega^2 + 1.5012\omega + 0.3417 \\ m_2 = 0 \\ m_3 = 0.49 \end{gathered} \tag{B.1}$$

In Fig. B.1 is displayed the correlation relating the alpha function parameter m_1 to the acentric factor ω.

C. Supplementary content

Supplementary content related to this article can be found in the attached word file.

References

[1] V. Lasserre, F. Heyndrickx, R. Rivoallon, and L. Guegan, “le règlement F-Gas, objectifs et impacts,” *Rev. Générale du Froid du Cond. d’Air*, 2014.

[2] B. Minor and M. Spatz, “HFO-1234yf Low GWP Refrigerant Update,” *International Refrigeration and Air Conditioning Conference*. 2008.

[3] J. D. Waals, *Over de continuiteit van den gas- en vloeistoftoestand*. A. W. Sijthoff, 1873.

[4] J. V. Sengers, R. F. Kayser, C. J. Peters, and H. J. White, *Equations of State for Fluids and Fluid Mixtures*. Elsevier, 2000.

[5] J. O. Valderrama, “The State of the Cubic Equations of State,” *Ind. Eng. Chem. Res.*, vol. 42, no. 8, pp. 1603–1618, Apr. 2003.

[6] Y. S. Wei and R. J. Sadus, “Equations of state for the calculation of fluid-phase equilibria,” *AIChE J.*, vol. 46, no. 1, pp. 169–196, Jan. 2000.

[7] C. H. Twu, J. E. Coon, and J. R. Cunningham, “A new cubic equation of state,” *Fluid Phase Equilib.*, vol. 75, pp. 65–79, Aug. 1992.

[8] C. H. Twu, D. Bluck, J. R. Cunningham, and J. E. Coon, “A cubic equation of state with a new alpha function and a new mixing rule,” *Fluid Phase Equilib.*, vol. 69, pp. 33–50, Dec. 1991.

[9] H. Orbey and S. I. Sandler, *Modeling Vapor-Liquid Equilibria: Cubic Equations of State and Their Mixing Rules, Volume 1*. Cambridge University Press, 1998.

[10] W.-R. Ji and D. A. Lempe, “A systematic study of cubic three-parameter equations of state for deriving a structurally optimized PVT relation,” *Fluid Phase Equilib.*, vol. 147, no. 1–2, pp. 85–103, Jun. 1998.

[11] A. Péneloux, E. Rauzy, and R. Fréze, “A consistent correction for Redlich-Kwong-Soave volumes,” *Fluid Phase Equilib.*, vol. 8, no. 1, pp. 7–23, Jan. 1982.

[12] J.-N. Jaubert, R. Privat, Y. L. E. Guennec, and L. Coniglio, “Note on the properties altered by application of a Péneloux–type volume translation to an equation of state,” *Fluid Phase Equilib.*, vol. 419, pp. 88–95, Mar. 2016.

[13] H. Segura, D. Seiltgens, A. Mejía, F. Llovell, and L. F. Vega, “An accurate direct technique for parameterizing cubic equations of state,” *Fluid Phase Equilib.*, vol. 265, no. 1–2, pp. 155–172, Mar. 2008.

[14] M. M. Abbott, “Cubic equations of state,” *AIChE J.*, vol. 19, no. 3, pp. 596–601, May 1973.

[15] G. Schmidt and H. Wenzel, “A modified van der Waals type equation of state,” *Chem. Eng. Sci.*, vol. 35, no. 7, pp. 1503–1512, Jan. 1980.

[16] N. C. Patel and A. S. Teja, “A new cubic equation of state for fluids and fluid mixtures,” *Chem. Eng. Sci.*, vol. 37, no. 3, pp. 463–473, 1982.

[17] J. O. Valderrama, “A generalized Patel-Teja equation of state for polar and nonpolar fluids and their mixtures.,” *J. Chem. Eng. JAPAN*, vol. 23, no. 1, pp. 87–91, Mar. 1990.

[18] A. Danesh, D.-H. Xu, and A. C. Todd, “Comparative study of cubic equations of state for predicting phase behaviour and volumetric properties of injection gas-reservoir oil systems,” *Fluid Phase Equilib.*, vol. 63, no. 3, pp. 259–278, 1991.

[19] L. A. Forero G. and J. A. Velásquez J., “The Patel–Teja and the Peng–Robinson EoSs performance when Soave alpha function is replaced by an exponential function,” *Fluid Phase Equilib.*, vol. 332, pp. 55–76, Oct. 2012.

[20] W.-R. Ji, E. Stiebing, G. Hradetzky, and D. A. Lempe, “Extrapolation of VLE data and simultaneous representation of caloric and volumetric properties by means of a cubic 3-parameter equation of state,” *Fluid Phase Equilib.*, vol. 260, no. 1, pp. 113–125, Oct. 2007.

[21] P. M. Mathias and T. W. Copeman, “Extension of the Peng-Robinson equation of state to complex mixtures: Evaluation of the various forms of the local composition concept,” *Fluid Phase Equilib.*, vol. 13, pp. 91–108, Jan. 1983.
[22] E. W. Lemmon, M. L. Huber, and M. O. McLinden, “REFPROP, Reference Fluid Thermodynamic and Transport Properties.” 2010.
[23] A. Valtz, H. Madani, C. Coquelet, and D. Richon, “Arkema Confidential Report,” 2008.
[24] K. Tanaka and Y. Higashi, “Thermodynamic properties of HFO-1234yf (2,3,3,3-tetrafluoropropene),” *Int. J. Refrig.*, vol. 33, no. 3, pp. 474–479, 2010.
[25] C. Coquelet, D. Ramjugernath, H. Madani, A. Valtz, P. Naidoo, and A. H. Meniai, “Experimental Measurement of Vapor Pressures and Densities of Pure Hexafluoropropylene,” *J. Chem. Eng. Data*, vol. 55, no. 6, pp. 2093–2099, Jun. 2010.
[26] V. G. Niesen, L. J. Van Poolen, S. L. Outcalt, and C. D. Holcomb, “Coexisting densities and vapor pressures of refrigerants R-22, R-134a, and R-124 at 300–395 K,” *Fluid Phase Equilib.*, vol. 97, pp. 81–95, Jun. 1994.
[27] T. Y. Kwak and G. A. Mansoori, “Van der waals mixing rules for cubic equations of state. Applications for supercritical fluid extraction modelling,” *Chem. Eng. Sci.*, vol. 41, no. 5, pp. 1303–1309, Jan. 1986.
[28] C.-N. Kim and Y.-M. Park, “Vapor–Liquid Equilibrium of HFC-32/134a And HFC-125/134a Systems,” *Int. J. Thermophys.*, vol. 20, no. 2, pp. 519–530.
[29] J. S. Lim, J.-Y. Park, B.-G. Lee, and Y.-W. Lee, “Phase equilibria of 1,1,1-trifluoroethane (HFC-143a) + 1,1,1,2-tetrafluoroethane (HFC-134a), and + 1,1-difluoroethane (HFC-152a) at 273.15, 293.15, 303.15, and 313.15 K,” *Fluid Phase Equilib.*, vol. 193, no. 1–2, pp. 29–39, Jan. 2002.
[30] Y. Higashi, “Vapor−Liquid Equilibrium, Coexistence Curve, and Critical Locus for Pentafluoroethane + 1,1,1-Trifluoroethane (R125/R143a),” *J. Chem. Eng. Data*, vol. 44, no. 2, pp. 333–337, Mar. 1999.
[31] C. Coquelet, D. Nguyen Hong, A. Chareton, A. Baba-Ahmed, and D. Richon, “Vapour–liquid equilibrium data for the difluoromethane+1,1,1,2,3,3,3-heptafluoropropane system at temperatures from 283.20 to 343.38 K and pressures up to 4.5 MPa,” *Int. J. Refrig.*, vol. 26, no. 5, pp. 559–565, Aug. 2003.
[32] E.-Y. Chung and M. S. Kim, “Vapor−Liquid Equilibria for the Difluoromethane (HFC-32) + 1,1,1,2-Tetrafluoroethane (HFC-134a) System,” *J. Chem. Eng. Data*, vol. 42, no. 6, pp. 1126–1128, Nov. 1997.
[33] P. Hu, L. X. Chen, and Z. S. Chen, “Vapor-liquid equilibria for the 1,1,1,2-tetrafluoroethane (HFC-134a)+1,1,1,2,3,3,3-heptafluoropropane (HFC-227ea) and 1,1,1-trifluoroethane (HFC-143a)+2,3,3,3-tetrafluoroprop-1-ene (HFO-1234yf) systems,” *Fluid Phase Equilib.*, vol. 360, pp. 293–297, 2013.
[34] A. Valtz, C. Coquelet, and D. Richon, “Vapor–Liquid Equilibrium Data for the Sulfur Dioxide (SO 2) + Difluoromethane (R32) System at Temperatures from 288.07 to 403.16 K and at Pressures up to 7.31 MPa,” *Int. J. Thermophys.*, vol. 25, no. 6, pp. 1695–1711, Nov. 2004.
[35] F. Rivollet, A. Chapoy, C. Coquelet, and D. Richon, “Vapor–liquid equilibrium data for the carbon dioxide (CO2) + difluoromethane (R32) system at temperatures from 283.12 to 343.25 K and pressures up to 7.46 MPa,” *Fluid Phase Equilib.*, vol. 218, no. 1, pp. 95–101, Apr. 2004.
[36] Y. Zhang, M. Gong, and J. Wu, “Vapor-liquid equilibrium measurement and correlation for R23 + R116 system,” *J. Chem. Ind. Eng.*, vol. 59, pp. 269–275, 2008.
[37] E. El Ahmar, A. Valtz, P. Paricaud, C. Coquelet, L. Abbas, and W. Rached, “Vapour–liquid equilibrium of binary systems containing pentafluorochemicals from 363 to

413 K: Measurement and modelling with Peng–Robinson and three SAFT-like equations of states," *Int. J. Refrig.*, vol. 35, no. 8, pp. 2297–2310, Dec. 2012.
[38] M. Ju, Y. Yun, M. S. Shin, and H. Kim, "(Vapour+liquid) equilibria of the {trifluoromethane (HFC-23)+propane} and {trifluoromethane (HFC-23)+n-butane} systems," *J. Chem. Thermodyn.*, vol. 41, no. 12, pp. 1339–1342, Dec. 2009.
[39] J.-N. Jaubert and F. Mutelet, "VLE predictions with the Peng–Robinson equation of state and temperature dependent kij calculated through a group contribution method," *Fluid Phase Equilib.*, vol. 224, no. 2, pp. 285–304, Oct. 2004.
[40] J.-N. Jaubert, S. Vitu, F. Mutelet, and J.-P. Corriou, "Extension of the PPR78 model (predictive 1978, Peng–Robinson EOS with temperature dependent kij calculated through a group contribution method) to systems containing aromatic compounds," *Fluid Phase Equilib.*, vol. 237, no. 1–2, pp. 193–211, Oct. 2005.
[41] R. Privat, J.-N. Jaubert, and F. Mutelet, "Use of the PPR78 Model To Predict New Equilibrium Data of Binary Systems Involving Hydrocarbons and Nitrogen. Comparison with Other GCEOS," *Ind. Eng. Chem. Res.*, vol. 47, no. 19, pp. 7483–7489, Oct. 2008.
[42] S. Vitu, R. Privat, J.-N. Jaubert, and F. Mutelet, "Predicting the phase equilibria of CO2+hydrocarbon systems with the PPR78 model (PR EOS and kij calculated through a group contribution method)," *J. Supercrit. Fluids*, vol. 45, no. 1, pp. 1–26, May 2008.
[43] J.-N. Jaubert, R. Privat, and F. Mutelet, "Predicting the phase equilibria of synthetic petroleum fluids with the PPR78 approach," *AIChE J.*, vol. 56, no. 12, pp. 3225–3235, Dec. 2010.
[44] K. Wilson, "Renormalization Group and Critical Phenomena. II. Phase-Space Cell Analysis of Critical Behavior," *Phys. Rev. B*, vol. 4, no. 9, pp. 3184–3205, Nov. 1971.
[45] K. Wilson and M. Fisher, "Critical Exponents in 3.99 Dimensions," *Phys. Rev. Lett.*, vol. 28, no. 4, pp. 240–243, Jan. 1972.
[46] M. Dicko and C. Coquelet, "Application of a new crossover treatment to a generalized cubic equation of state," *Fluid Phase Equilib.*, vol. 302, no. 1–2, pp. 241–248, Mar. 2011.
[47] J. Janeček, P. Paricaud, M. Dicko, and C. Coquelet, "A generalized Kiselev crossover approach applied to Soave–Redlich–Kwong equation of state," *Fluid Phase Equilib.*, vol. 401, pp. 16–26, Sep. 2015.
[48] J. Cai and J. M. Prausnitz, "Thermodynamics for fluid mixtures near to and far from the vapor–liquid critical point," *Fluid Phase Equilib.*, vol. 219, no. 2, pp. 205–217, May 2004.
[49] M. L. Huber, D. G. Friend, and J. F. Ely, "Prediction of the thermal conductivity of refrigerants and refrigerant mixtures," *Fluid Phase Equilib.*, vol. 80, pp. 249–261, Nov. 1992.
[50] S. . Klein, M. . McLinden, and A. Laesecke, "An improved extended corresponding states method for estimation of viscosity of pure refrigerants and mixtures," *Int. J. Refrig.*, vol. 20, no. 3, pp. 208–217, May 1997.

List of tables

List of figures

Fig. 8 - VLE prediction for R-143a (1) + R-134a (2). Experimental data [29]**: (●) 273.15K; (▲) 293.15K; (×) 303.15 K; (Δ) 313.15 K. NEoS: (——) k_{ij} = 0.**

Fig. 9 - VLE prediction for R-125 (1) + R-143a (2). Experimental data [30]**: (●) 273.15 K; (▲) 293.15 K; (×) 313.15 K. NEoS: (——) k_{ij} = 0.**

Fig. 10 - VLE prediction for R-32 (1) + R-227ea (2). Experimental data [31]**: (●) 283.20 K; (▲) 303.21 K; (×) 323.21 K; (Δ) 343.38 K. NEoS: (——) k_{ij} = 0.**

Fig. 11 - VLE prediction for R-32 (1) + R-134a (2). Experimental data [32]**: (●) 263.15 K; (▲) 273.15 K; (×) 283.15 K; (Δ) 293.15 K; (□) 303.15 K; (○) 313.15 K; (+) 323.15 K. NEoS: (——) k_{ij} = 0**

Fig. 12 - VLE prediction for R-143a (1) + R-1234yf (2). Experimental data [33]**: (●) 283.15 K; (▲) 293.15 K; (×) 303.15 K; (Δ) 313.15 K; (□) 323.15 K. NEoS: (——) k_{ij} = 0.**

Fig. 13 - VLE prediction for SO_2 (1)+ R-32 (2). Experimental data [34]**: (●) 288.07 K; (▲) 303.16 K; (×) 323.15 K; (Δ) 343.15 K; (□) 353.15 K; (○) 363.15 K; (+) 383.18 K; (■) 403.16 K. NEoS: (——) k_{ij} = 0; (- - - -) k_{ij} adjusted.**

Fig. 14 - VLE prediction for CO_2 (1) + R-32 (2). Experimental data [35]**: (●) 283.12 K; (▲) 293.11 K; (×) 303.13 K; (Δ) 305.15 K; (□) 313.30 K; (○) 323.34 K; (+) 333.33 K; (■) 343.23 K. NEoS: (——) k_{ij} = 0; (- - - -) k_{ij} adjusted.**

Fig. 15 - VLE prediction for R-23 (1) + R-116 (2). Experimental data [36]**: (●) 194.33 K; (▲) 199.71 K; (×) 214.19 K; (Δ) 229.63 K; (□) 244.94 K. NEoS: (——) k_{ij} = 0; (- - - -) k_{ij} adjusted.**

Fig. 16 - VLE prediction for isopentane (1) + R-365mfc (2). Experimental data [37]**: (●) 363.12 K; (▲) 373.20 K; (×) 393.22 K; (Δ) 413.09 K. NEoS: (——) k_{ij} = 0; (- - - -) k_{ij} adjusted.**

Fig. 17 - VLE prediction for R-23 (1) + butane (2). Experimental data [38]**: (●) 283.15 K; (▲) 293.15 K; (×) 303.15 K; (Δ) 313.15 K. NEoS: (——) k_{ij} = 0; (- - - -) k_{ij} adjusted.**

Fig. 18 - VLE prediction for isopentane (1) + R-245fa (2). Experimental data [37]**: (●) 362.94 K; (▲) 373.17 K; (×) 392.87 K; (Δ) 412.91 K. NEoS: (——) k_{ij} = 0; (- - - -) k_{ij} adjusted.**

Fig. 19 - P-ρ diagram for R-421A. (——) REFPROP; (×) Critical Point: REFPROP (T_c = 355.93 K); (- - - -) NEoS; (……) PT-EoS; (— — —) PR-EoS. Out of saturation: T_r = 0.7, 0.9, 1.0, 1.1.

Fig. 20 - P-ρ diagram for R-508A. (——) REFPROP; (×) Critical Point: REFPROP (T_c = 283.34K); (- - - -) NEoS; (……) PT-EoS; (— — —) PR-EoS. Out of saturation: T_r = 0.7, 0.9, 1.0, 1.1.

Fig. 21 - P-ρ diagram for R-404A. (——) REFPROP; (×) Critical Point: REFPROP (T_c=345.2 K); (- - - -) NEoS; (……) PT-EoS; (— — —) PR-EoS. Out of saturation: T_r = 0.7, 0.9, 1.0, 1.1.

Fig. A.1 - Correlations obtained with the PT-EoS. (a): the m_1 parameter as a function of the acentric factor ω (coefficient of determination R^2 = 0.83). (b): the optimized critical compressibility factor $Z_{c,opt}$ as a function of the experimental critical compressibility factor Z_c (coefficient of determination R^2 = 0.92).

Fig. B.1 - Correlation obtained with the PR-EoS: m_1 parameter as a function of the acentric factor ω (coefficient of determination R^2 = 0.98).

Fig. C.1 - k_{ij} as a function of temperature: CO_2 + R-32. (●) NEoS; (▲) PR-EoS;(- - - -) CO_2 critical temperature (T_c = 304.13 K).

Fig. C.2– k_{ij} as a function of temperature: SO_2 + R-32. (●) NEoS; (▲) PR-EoS;(- - - -) R-32 critical temperature (T_c = 351.26 K).

Fig. C.3 - k_{ij} as a function of temperature: isopentane + R-365mfc. (●) NEoS; (▲) PR-EoS.

Fig. C.4- k_{ij} as a function of temperature: R-23 + R-116. (●) NEoS; (▲) PR-EoS.

Fig. C.5 - k_{ij} as a function of temperature: isopentane + R-245fa. (●) NEoS; (▲) PR-EoS.

Fig. C.6 - k_{ij} as a function of temperature: R-23 + butane. (●) NEoS; (▲) PR-EoS.

Fig. C.7 - Enthalpies of saturated phases. (○) REFPROP. (- - - -) NEoS.

Fig. C.8 - Enthalpies of vaporization. (○) REFPROP. (- - - -) NEoS.

Fig. C.9 – Isobaric heat capacities of saturated phases. (○) Liquid. (●) Vapor – REFPROP. (- - - -) NEoS.

Fig. C.10 – Isobaric heat capacities at P = 5 MPa. (○) REFPROP. (- - - -) NEoS.

Table 5 - Experimental and NEoS adjusted parameters for several refrigerant families (with m_2 = 0.47 and m_3 = -0.08). ω is the acentric factor, m_1 the alpha function parameter, and $Z_{c,opt}$ and Z_c the optimized and the experimental critical compressibility factors, respectively.

Families	Compounds	ω	m_1	$Z_{c,opt}$	Z_c
PFC	R-C318	0.35530	0.60916	0.29152	0.27751
	R-14	0.17850	0.39304	0.29695	0.27883
	R-116	0.25660	0.49092	0.29399	0.28151
	R-218	0.31720	0.53351	0.28765	0.27553
CFC	R-11	0.18875	0.36197	0.28744	0.27901
	R-12	0.17948	0.34391	0.28682	0.27643
	R-13	0.17230	0.34292	0.28839	0.27685
	R-113	0.25253	0.45677	0.28711	0.28019
	R-114	0.25230	0.47429	0.29044	0.27563
	R-115	0.25000	0.45928	0.29007	0.26779
HCFC	R-21	0.20610	0.38831	0.28473	0.27006
	R-22	0.22082	0.37537	0.27902	0.26825
	R-123	0.28192	0.46712	0.28022	0.26806
	R-124	0.28810	0.47540	0.28121	0.26865
	R-141b	0.21950	0.39624	0.28235	0.27057
	R-142b	0.23210	0.39073	0.27830	0.26786
HFC	R-125	0.30520	0.51102	0.28365	0.26844
	R-134a	0.32684	0.49929	0.27428	0.26004
	R-143a	0.26150	0.39374	0.26895	0.25502
	R-152a	0.27521	0.38981	0.26439	0.25233
	R-161	0.21700	0.33583	0.26915	0.25979
	R-227ea	0.35700	0.57089	0.28239	0.26849
	R-23	0.26300	0.39189	0.26924	0.25821
	R-236ea	0.37940	0.62687	0.28904	0.27578
	R-236fa	0.37721	0.59681	0.28170	0.26664
	R-245ca	0.35360	0.57228	0.28505	0.27003
	R-245fa	0.37760	0.59424	0.28041	0.26702
	R-32	0.27690	0.34346	0.25255	0.24291
	R-365mfc	0.38000	0.60464	0.28564	0.26686
	R-41	0.20040	0.25742	0.25587	0.24036
HFO	R-1234yf	0.27600	0.46360	0.28085	0.26519
	R-1234ze(E)	0.31300	0.50226	0.28049	0.26651
HCFO	R-1233zd(E)	0.34137	0.51623	0.28252	0.27884
NATURAL FLUIDS	CO_2	0.22394	0.42919	0.28868	0.27458

Table 6 - Calculated parameters for the R-1234yf, R-1216, CO2, R-125, R-134a, R-143a, R23 and R-116 (m_2 and m_3 are set to fixed values).

CEoS	Compound	m_1	m_2	m_3	$Z_{c,opt}$
NEoS	R-1234yf	0.44741	0.47	-0.08	0.27917
	R-1216	0.56391	0.47	-0.08	0.28529
	CO_2	0.38725	0.47	-0.08	0.28714
	R-125	0.48777	0.47	-0.08	0.28208
	R-134a	0.52074	0.47	-0.08	0.27424
	R-143a	0.42914	0.47	-0.08	0.26906
	R-23	0.43097	0.47	-0.08	0.27239
	R-116	0.42322	0.47	-0.08	0.29217
PT-EoS	R-1234yf	0.73498	-0.01	0.4	0.30417
	R-1216	0.86744	-0.01	0.4	0.30979
	CO_2	0.66975	-0.01	0.4	0.31139
	R-125	0.78021	-0.01	0.4	0.30689
	R-134a	0.81773	-0.01	0.4	0.29936
	R-143a	0.71483	-0.01	0.4	0.29409
	R-23	0.71684	-0.01	0.4	0.29750
	R-116	0.70837	-0.01	0.4	0.31543
PR-EoS	R-1234yf	0.74884	0	0.49	0.30740[a]
	R-1216	0.85972	0	0.49	0.30740
	CO_2	0.67314	0	0.49	0.30740
	R-125	0.79107	0	0.49	0.30740
	R-134a	0.82227	0	0.49	0.30740
	R-143a	0.72781	0	0.49	0.30740
	R-23	0.72999	0	0.49	0.30740
	R-116	0.72069	0	0.49	0.30740

[a] For the PR-EoS, the value of Z_c is set to 0.30740.

Table 7 – ARD and BIAS for R-1234yf using the adjusted parameters for EoSs

	ARD (%)			BIAS (%)		
CEoS	**P**	**ρ^L**	**ρ^V**	**P**	**ρ^L**	**ρ^V**
NEoS	0.4	1.9	2.0	-0.2	0.2	-1.5
PT-EoS	0.5	4.3	0.9	-0.3	0.5	0.1
PR-EoS	0.9	3.9	0.8	-0.5	3.3	0.2

Table 8.a - ARD and BIAS for the pure compounds R-1234yf, R-1216, CO2, R-134a, the binary mixtures R-421A, R-508A, and the ternary mixture R-404A, using the calculated parameters for EoSs.

		ARD (%)			BIAS (%)		
Compounds	**CEoS**	**P**	**ρ^L**	**ρ^V**	**P**	**ρ^L**	**ρ^V**
R-1234yf	**NEoS**	1.4	2.2	2.9	-1.4	-0.6	-2.8
	PT-EoS	2.2	3.9	2.0	-2.2	1.9	-1.8
	PR-EoS	1.9	3.9	1.6	-1.9	3.4	-1.3
R-1216	**NEoS**	0.5	5.2	6.2	-0.5	4.0	-4.9
	PT-EoS	0.9	9.9	3.2	-0.9	9.4	-0.8
	PR-EoS	0.6	9.5	3.5	-0.6	8.4	-0.8
CO_2	**NEoS**	2.7	2.3	5.9	-2.7	-0.2	-5.6
	PT-EoS	3.0	4.4	3.9	-3.0	3.7	-3.2
	PR-EoS	1.4	4.3	2.1	-1.3	1.5	-1.5
R-134a	**NEoS**	4.4	2.8	5.5	4.4	-0.1	4.1
	PT-EoS	3.6	3.3	4.6	3.6	0.4	4.5
	PR-EoS	1.7	4.6	1.0	-1.0	4.6	0.0
R-421A	**NEoS**	1.1	2.4	23.2	-0.4	-1.8	-23.2
	PT-EoS	1.5	3.6	22.7	-1.4	0.5	-22.7
	PR-EoS	1.4	3.3	22.2	-1.3	2.5	-22.2
R-508A	**NEoS**	1.0	1.7	1.7	-0.4	-1.1	1.0
	PT-EoS	1.9	2.7	5.3	1.0	0.4	4.9
	PR-EoS	2.9	2.8	8.6	2.9	-0.4	8.6
R-404A	**NEoS**	1.6	2.3	5.8	-1.6	-1.1	-5.8
	PT-EoS	2.6	3.7	5.3	-2.6	1.3	-5.3
	PR-EoS	4.7	5.4	6.6	-4.7	5.4	-6.6

Table 4.b - ARD and BIAS of the pressure and vapor composition for the VLE calculation

Systems	T/K	k_{ij}	ARD (%)		BIAS (%)	
			P	y_1	P	y_1
R-125 (1) + R-134a (2)	**263.15**	0	1.5	1.2	0.0	-1.2
	273.15		1.2	1.1	0.1	-1.0
	283.15		1.1	1.1	0.3	-0.2
	293.15		0.9	1.4	0.2	-0.4
	303.15		0.7	1.1	0.4	-0.3
R-143a (1) + R-134a (2)	**273.15**	0	4.6	1.2	4.6	-0.8
	293.15		2.1	1.3	2.1	-1.3
	303.15		1.3	1.3	1.3	-1.3
	313.15		0.7	0.7	0.7	-0.7
R-125 (1) + R-143a (2)	**273.15**	0	1.9	3.0	1.0	-2.8
	293.15		1.1	1.6	0.5	-1.6
	313.15		0.7	1.2	0.3	-1.0
R-32 (1) + R-227ea (2)	**283.20**	0	4.7	1.6	4.6	1.6
	303.21		3.8	1.9	3.8	1.8
	323.21		3.5	2.0	3.5	2.0
	343.38		2.7	2.8	2.6	2.8
R-32 (1) + R-134a (2)	**263.15**	0	7.7	1.7	7.7	1.7
	273.15		6.2	0.9	6.2	0.9
	283.15		5.8	0.5	5.8	0.1
	293.15		4.5	1.0	4.5	-0.4
	303.15		3.7	0.6	3.7	0.1
	313.15		2.9	0.6	2.9	0.3
	323.15		2.1	0.6	2.1	0.3
R-143a (1) + R-1234yf (2)	**283.15**	0	2.5	1.9	2.1	1.9
	293.15		2.2	1.9	1.8	1.9
	303.15		1.8	1.9	1.5	1.9
	313.15		1.4	1.6	1.1	1.6
	323.15		1.1	1.4	0.9	1.4
SO_2 (1) + R-32 (2)	***288.07***	*0*	*3.8*	*1.3*	*2.6*	*1.3*
	303.16		*3.2*	*1.2*	*2.3*	*1.2*
	323.15		*1.8*	*0.8*	*0.8*	*0.8*
	343.15		*1.0*	*0.4*	*-0.5*	*0.1*
	353.15		*1.1*	*0.7*	*-1.1*	*0.3*
	363.15		*4.8*	*2.6*	*2.2*	*2.0*
	383.18		*4.3*	*3.3*	*0.7*	*3.3*
	403.16		*4.5*	*8.3*	*1.9*	*8.3*
	288.07	Adjusted (cf Table C.1 in	3.6	1.3	1.8	0.9
	303.16		3.0	0.8	1.3	0.7

	323.15	the supplementary content for k_{ij} values)	1.8	0.7	0.7	0.7
	343.15		0.9	0.3	0.2	0.3
	353.15		0.5	0.7	0.1	0.7
	363.15		2.9	1.3	1.1	1.0
	383.18		3.6	3.7	2.2	3.7
	403.16		2.1	7.1	1.7	7.1
CO_2 (1) + R-32 (2)	***283.12***	*0*	*5.2*	*2.6*	*4.9*	*-2.6*
	293.11		*4.3*	*1.6*	*4.2*	*-1.5*
	303.13		*10.0*	*1.4*	*10.0*	*-0.1*
	305.15		*10.0*	*3.1*	*10.0*	*0.3*
	313.30		*18.5*	*7.0*	*18.5*	*4.4*
	323.34		*26.4*	*9.5*	*26.4*	*8.5*
	333.33		*26.0*	*8.1*	*26.0*	*7.7*
	343.23		*17.3*	*15.4*	*17.3*	*15.4*
	283.12	Adjusted (cf Table C.1 in the supplementary content for k_{ij} values)	5.5	2.4	5.2	-2.4
	293.11		4.0	1.8	3.8	-1.7
	303.13		9.1	2.0	9.1	-0.5
	305.15		9.9	3.2	9.9	0.2
	313.30		11.3	4.4	11.3	2.3
	323.34		24.9	10.4	24.9	7.2
	333.33		25.8	8.8	25.8	7.0
	343.23		17.3	15.4	17.3	15.4
R-23 (1) + R-116 (2)	***194.33***	*0*	*20.8*	*12.2*	*18.0*	*8.4*
	199.71		*20.0*	*12.8*	*17.5*	*8.8*
	214.19		*17.8*	*11.4*	*15.9*	*7.2*
	229.63		*16.5*	*9.5*	*15.0*	*4.6*
	244.94		*15.1*	*9.0*	*14.0*	*4.2*
	194.33	Adjusted (cf Table C.1 in the supplementary content for k_{ij} values)	2.4	2.8	-1.5	2.8
	199.71		2.3	2.6	-1.5	2.6
	214.19		1.8	2.5	-1.3	1.9
	229.63		1.2	2.0	-0.6	1.3
	244.94		1.0	2.1	-0.3	1.2
isopentane (1) + R-365mfc (2)	***363.12***	*0*	*18.8*	*20.7*	*18.8*	*13.6*
	373.20		*15.6*	*23.4*	*15.6*	*15.7*
	393.22		*13.6*	*20.3*	*13.6*	*13.7*
	413.09		*13.1*	*15.8*	*13.1*	*11.0*
	363.12	Adjusted (cf Table C.1 in the supplementary content for k_{ij} values)	1.0	2.1	-1.0	-2.0
	373.20		1.6	1.3	-1.4	-0.4
	393.22		1.3	0.9	-1.3	-0.4
	413.09		0.9	1.1	-0.9	1.0
R-23 (1) + butane (2)	***283.15***	*0*	*39.8*	*14.3*	*38.8*	*13.0*
	293.15		*39.8*	*14.0*	*38.9*	*12.8*

	303.15		*40.7*	*15.1*	*39.7*	*13.8*
	313.15		*38.6*	*19.9*	*37.7*	*18.4*
	283.15	Adjusted (cf Table C.1 in the supplementary content for k_{ij} values)	3.2	0.5	-0.8	0.5
	293.15		4.3	0.9	0.2	0.9
	303.15		3.2	1.3	-0.8	1.3
	313.15		2.8	2.1	-0.6	2.1
isopentane (1) + R-245fa (2)	***362.94***	*0*	*24.1*	*27.3*	*24.1*	*-2.3*
	373.17		*18.3*	*18.2*	*18.3*	*-0.2*
	392.87		*16.8*	*27.0*	*16.8*	*7.9*
	412.91		*16.3*	*15.1*	*16.3*	*6.3*
	362.94	Adjusted (cf Table C.1 in the supplementary content for k_{ij} values)	2.1	5.7	-1.6	-5.7
	373.17		3.3	6.6	-2.9	-6.6
	392.87		3.3	4.4	-3.0	-4.4
	412.91		4.1	3.5	0.9	-2.6

Table A.1 - Experimental and PT-EoS adjusted parameters for several refrigerant families (with m_2 = -0.01 and m_3 = 0.4). ω is the acentric factor, m_1 the alpha function parameter, and $Z_{c,opt}$ and Z_c the optimized and the experimental critical compressibility factors, respectively.

Families	Compounds	ω	m_1	$Z_{c,opt}$	Z_c
PFC	R-C318	0.35530	0.90709	0.31295	0.27751
	R-14	0.17850	0.67555	0.31954	0.27883
	R-116	0.25660	0.77577	0.31510	0.28151
	R-218	0.31720	0.84300	0.31391	0.27553
CFC	R-11	0.18875	0.65407	0.31346	0.27901
	R-12	0.17948	0.63489	0.31310	0.27643
	R-13	0.17230	0.63476	0.31484	0.27685
	R-113	0.25253	0.74834	0.31080	0.28019
	R-114	0.25230	0.74764	0.30981	0.27563
	R-115	0.25000	0.75177	0.31374	0.26779
	R-22	0.22082	0.66722	0.30519	0.26825
	R-123	0.28192	0.76770	0.30627	0.26806
	R-124	0.28810	0.77740	0.30741	0.26865
	R-141b	0.21950	0.69075	0.30842	0.27057
HFC	R-125	0.30520	0.80551	0.30706	0.26844
	R-134a	0.32684	0.79532	0.29871	0.26004
	R-143a	0.26150	0.67484	0.29264	0.25502
	R-152a	0.27521	0.67453	0.28916	0.25233
	R-161	0.21700	0.62261	0.29548	0.25979
	R-227ea	0.35700	0.88229	0.30851	0.26849
	R-23	0.26300	0.67957	0.29438	0.25821
	R-236ea	0.37940	0.92944	0.31120	0.27578
	R-236fa	0.37721	0.90641	0.30662	0.26664
	R-245ca	0.35360	0.87946	0.30986	0.27003
	R-245fa	0.37760	0.90658	0.30630	0.26702
	R-32	0.27690	0.61931	0.27683	0.24291
	R-365mfc	0.38000	0.90970	0.30914	0.26686
	R-41	0.20040	0.52412	0.27968	0.24036
HFO	R-1234yf	0.27600	0.74045	0.30169	0.26519
	R-1234ze(E)	0.31300	0.80128	0.30522	0.26651
HCFO	R-1233zd(E)	0.34137	0.82034	0.30811	0.27884

Table B.1 - Experimental and PR-EoS adjusted parameters for several refrigerant families (with $m_2 = 0$ and $m_3 = 0.49$). ω is the acentric factor, m_1 the alpha function parameter, and $Z_{c,opt}$ and Z_c the optimized and the experimental critical compressibility factors, respectively.

Families	Compounds	ω	m_1
PFC	R-C318	0.35530	0.87504
	R-14	0.17850	0.61886
	R-116	0.25660	0.73579
	R-218	0.31720	0.80385
CFC	R-11	0.18875	0.61810
	R-12	0.17948	0.59947
	R-13	0.17230	0.59317
	R-113	0.25253	0.72610
	R-114	0.25230	0.73275
	R-115	0.25000	0.71730
HCFC	R-21	0.20610	0.65949
	R-22	0.22082	0.66061
	R-123	0.28192	0.75902
	R-124	0.28810	0.76343
	R-141b	0.21950	0.67316
	R-142b	0.23210	0.68115
HFC	R-125	0.30520	0.79991
	R-134a	0.32684	0.82270
	R-143a	0.26150	0.72686
	R-152a	0.27521	0.73535
	R-161	0.21700	0.65300
	R-227ea	0.35700	0.86570
	R-23	0.26300	0.71889
	R-236ea	0.37940	0.90565
	R-236fa	0.37721	0.90003
	R-245ca	0.35360	0.85944
	R-245fa	0.37760	0.89974
	R-32	0.27690	0.72710
	R-365mfc	0.38000	0.89465
	R-41	0.20040	0.61788
HFO	R-1234yf	0.27600	0.76202
	R-1234ze(E)	0.31300	0.80066
HCFO	R-1233zd(E)	0.34137	0.80854
NATURAL FLUIDS	CO_2	0.22394	0.69219

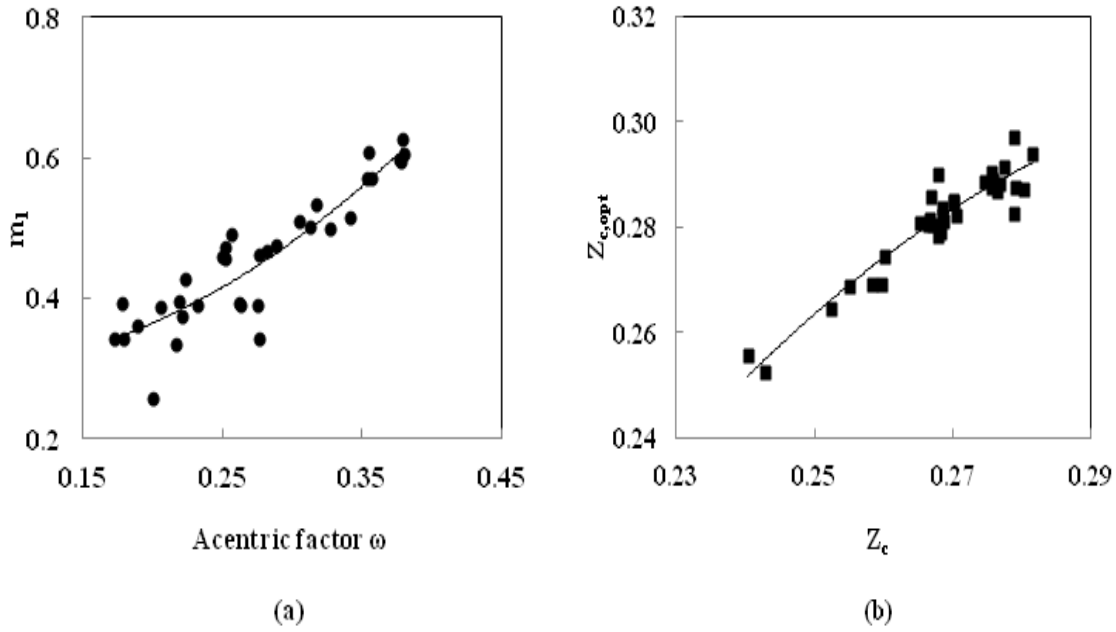

Fig. 22 - Correlations obtained with the NEoS. (a): the m_1 parameter as a function of the acentric factor ω (coefficient of determination $R^2 = 0.82$); (b): the optimized critical compressibility factor $Z_{c,opt}$ as a function of the experimental critical compressibility factor Z_c (coefficient of determination $R^2 = 0.89$).

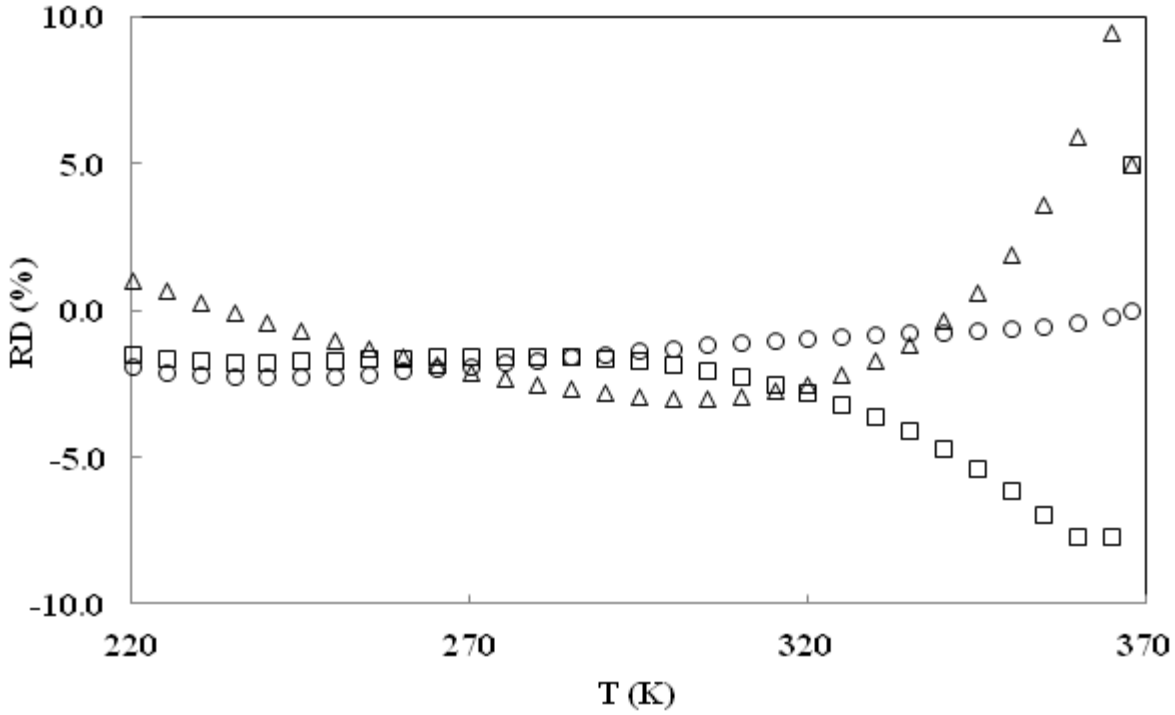

Fig. 23 – Relative deviation (RD) as a function of the temperature for R-1234yf with NEoS, using the calculated parameters.
(○) RD of vapor pressure; (Δ) RD of saturated liquid density;
(□) RD of saturated vapor density.

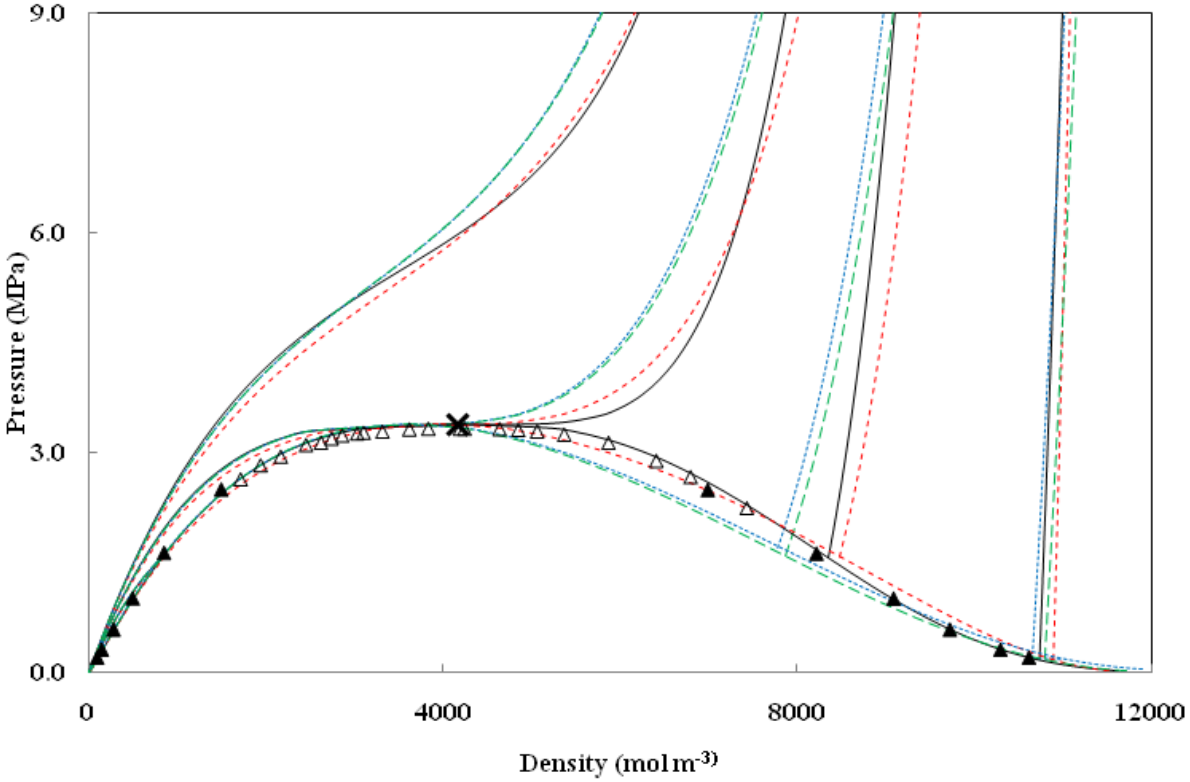

Fig. 24 - P-ρ diagram for R-1234yf.
(Δ) Experimental data [24]; **(▲) Confidential Experimental data** [23]; **(——) REFPROP; (×) Critical Point: REFPROP (T_c = 367.85K); (- - - -) NEoS; (……) PT-EoS; (— — —) PR-EoS. Out of saturation: T_r = 0.7, 0.9, 1.0, 1.1.**

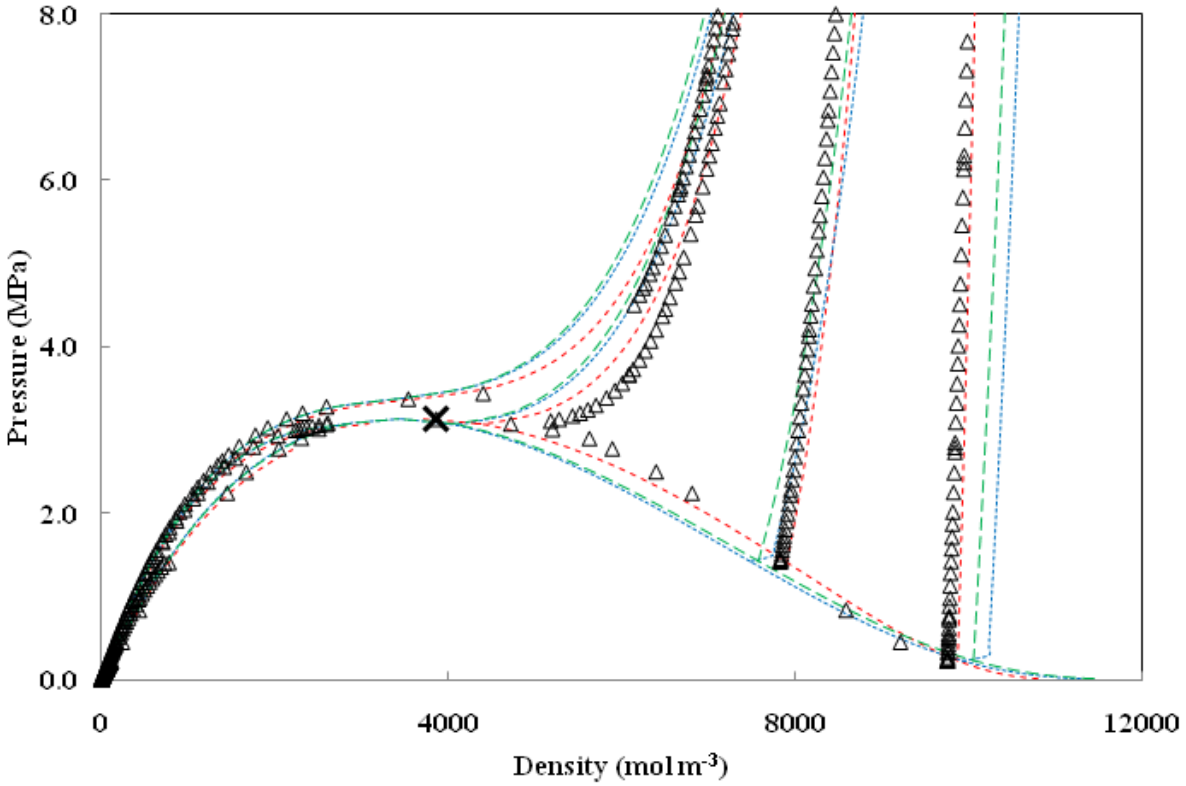

Fig. 25 - P-ρ diagram for R-1216.
(Δ) Experimental data [25]; **(×) Critical Point: Experimental (T_c=358.9 K)** [25]; **(- - - -) NEoS; (.....) PT-EoS; (— — —) PR-EoS. Out of saturation: T_r = 0.73, 0.9, 1.0, and 1.01.**

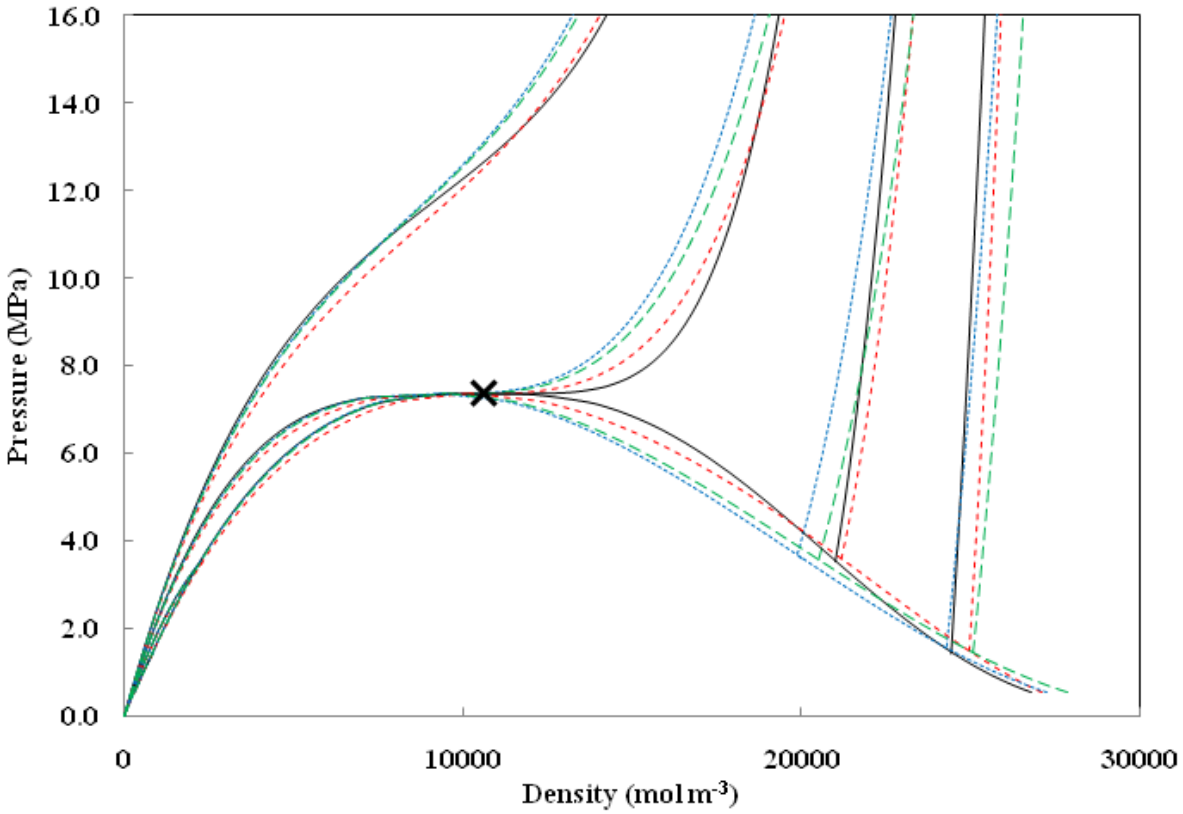

Fig. 26 - P-ρ diagram for CO_2.
(——) REFPROP; (×) Critical Point: REFPROP (T_c=304.13K); (- - - -) NEoS; (……) PT-EoS; (– – –) PR-EoS. Out of saturation: T_r = 0.8, 0.9, 1.0, and 1.1.

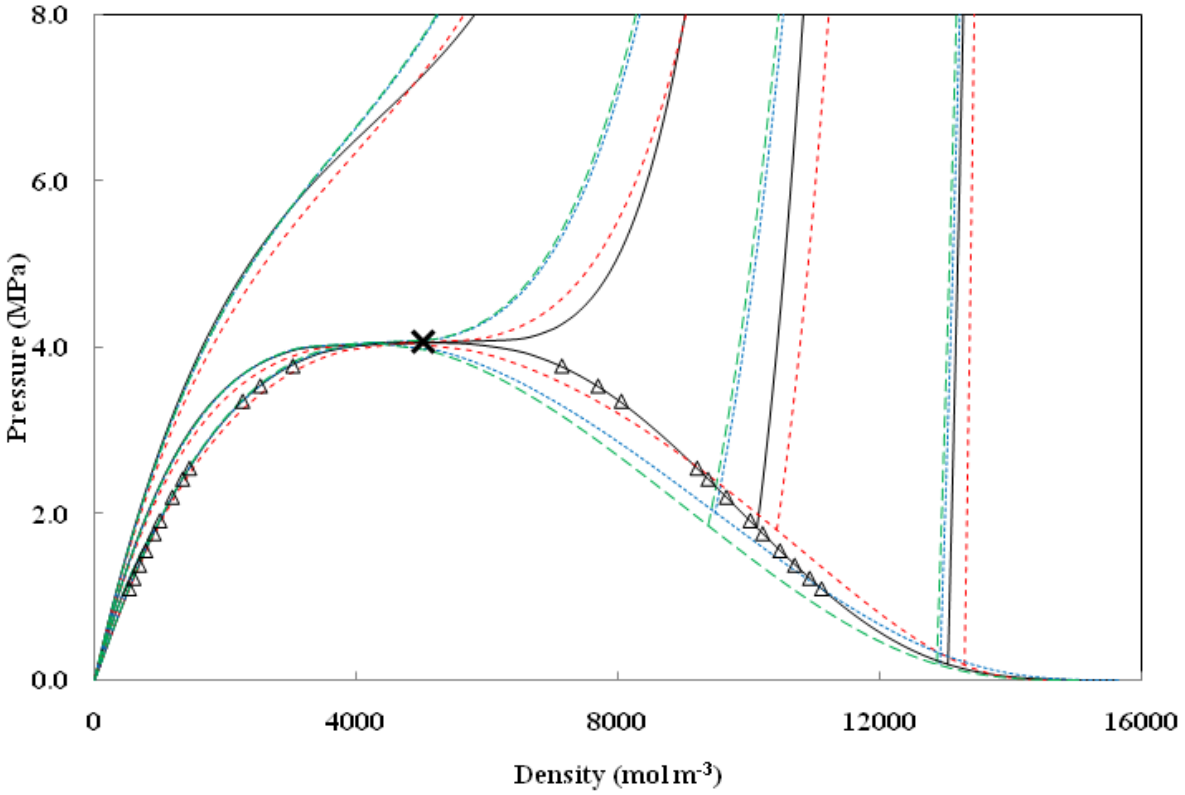

Fig. 27 - P-ρ diagram for R-134a.
(Δ) Experimental data [26]; **(——) REFPROP; (×) Critical Point: REFPROP (T_c=374.21K); (- - - -) NEoS; (.....) PT-EoS; (— — —) PR-EoS. Out of saturation: T_r = 0.7, 0.9, 1.0, and 1.**

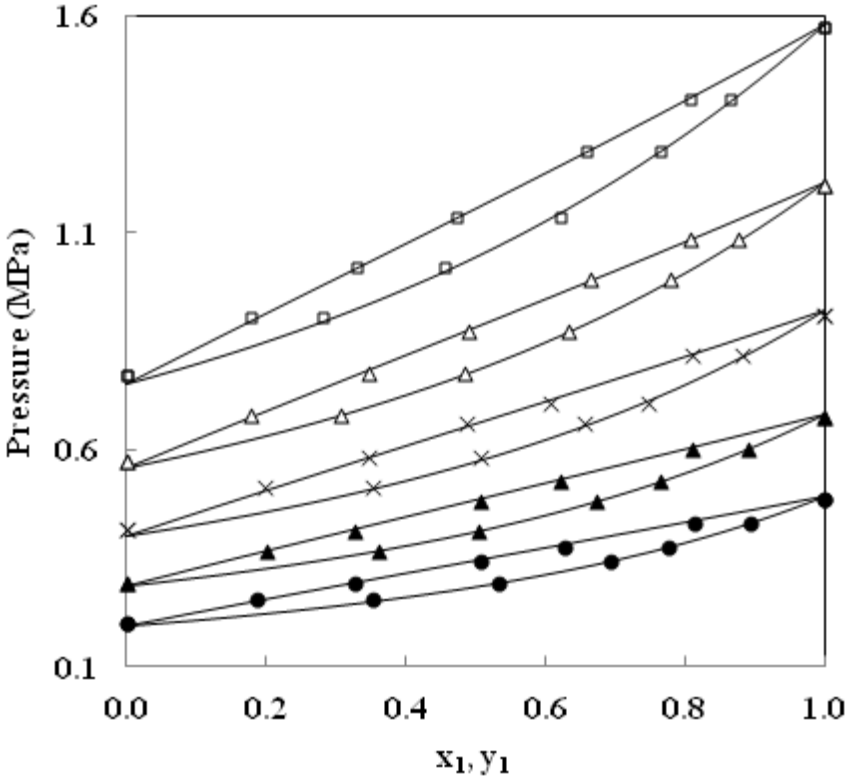

Fig. 28 - VLE prediction for R-125 (1) + R-134a (2).
Experimental data [28]**: (●) 263.15 K; (▲) 273.15 K;**
(×) 283.15 K; (Δ) 293.15 K; (□) 303.15 K.
NEoS: (—) k_{ij} = 0.

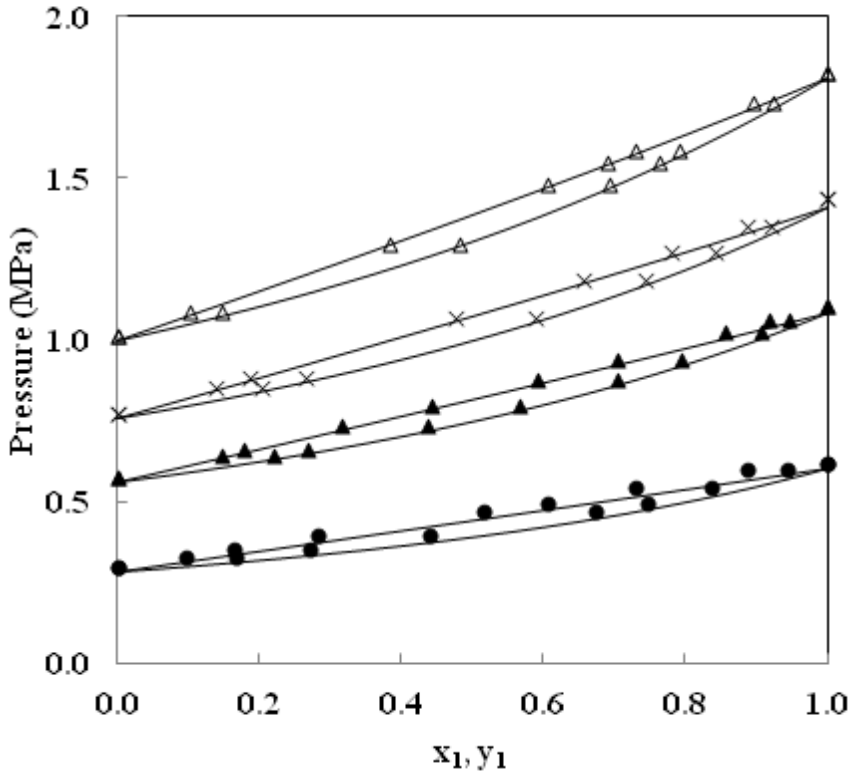

Fig. 29 - VLE prediction for R-143a (1) + R-134a (2).
Experimental data [29]**: (●) 273.15K; (▲) 293.15K;**
(×) 303.15 K; (∆) 313.15 K.
NEoS: (—) k_{ij} = 0.

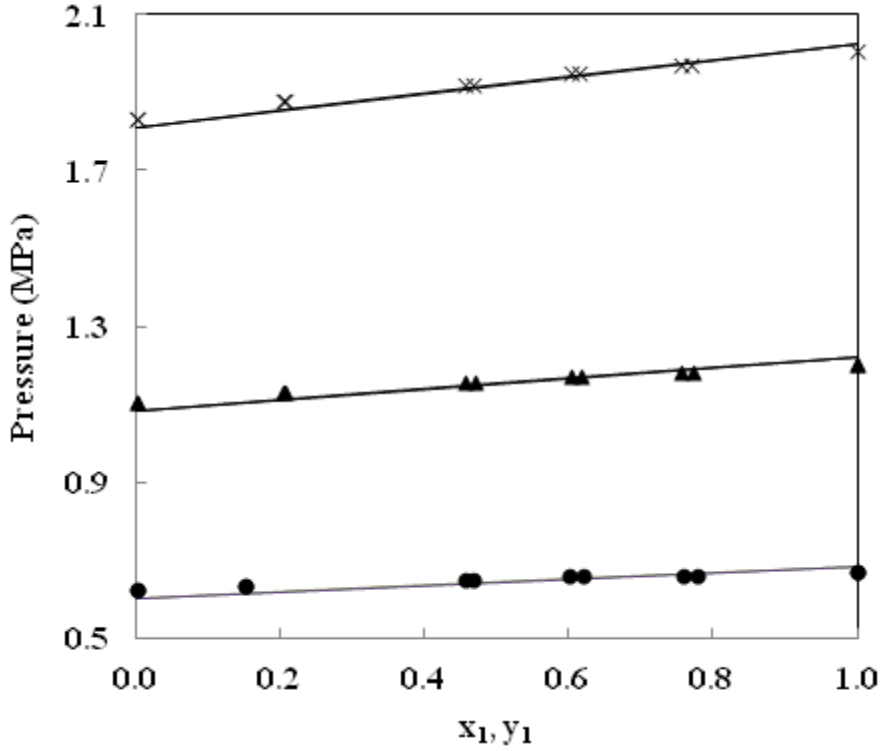

Fig. 30 - VLE prediction for R-125 (1) + R-143a (2). Experimental data [30]**: (●) 273.15 K; (▲) 293.15 K; (×) 313.15 K.**
NEoS: (—) k_{ij} = 0.

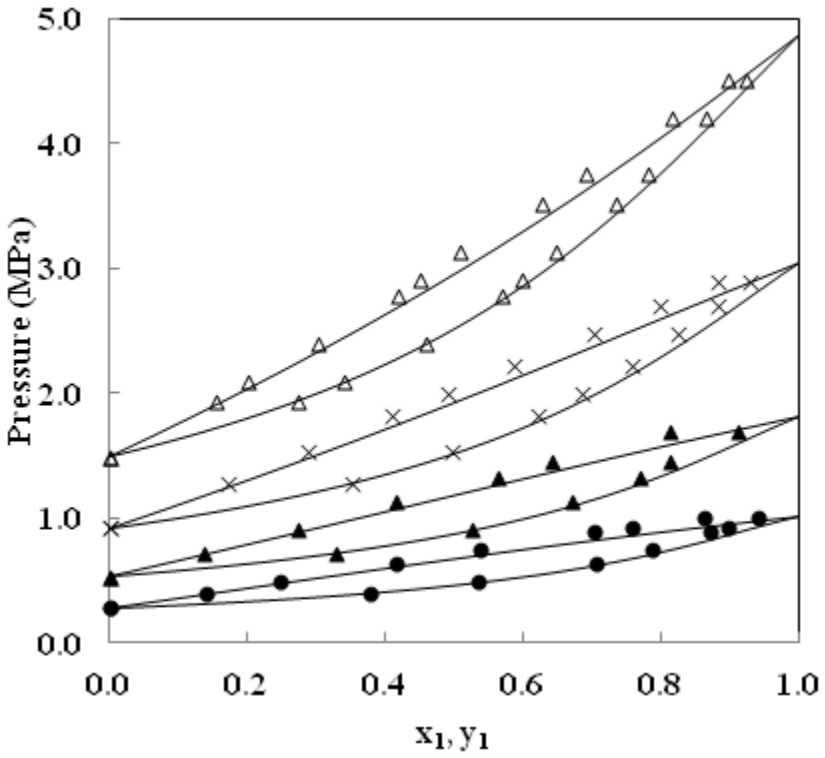

Fig. 31 - VLE prediction for R-32 (1) + R-227ea (2). Experimental data [31]**: (●) 283.20 K; (▲) 303.21 K; (×) 323.21 K; (Δ) 343.38 K. NEoS: (——) k_{ij} = 0.**

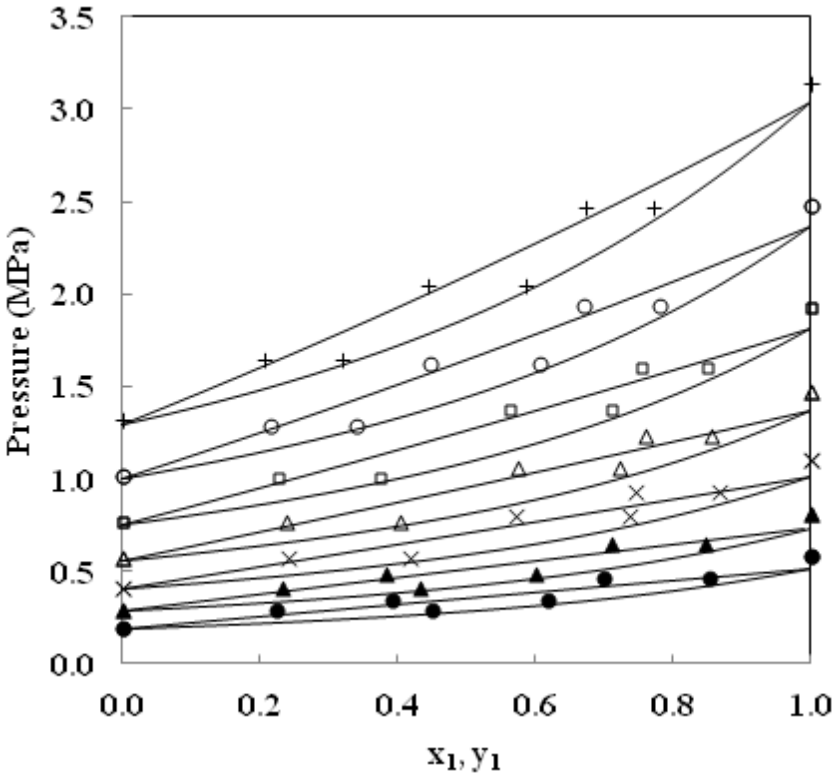

Fig. 32 - VLE prediction for R-32 (1) + R-134a (2). Experimental data [32]**: (●) 263.15 K; (▲) 273.15 K; (×) 283.15 K; (∆) 293.15 K; (□) 303.15 K; (○) 313.15 K; (+) 323.15 K. NEoS: (——) k_{ij} = 0.**

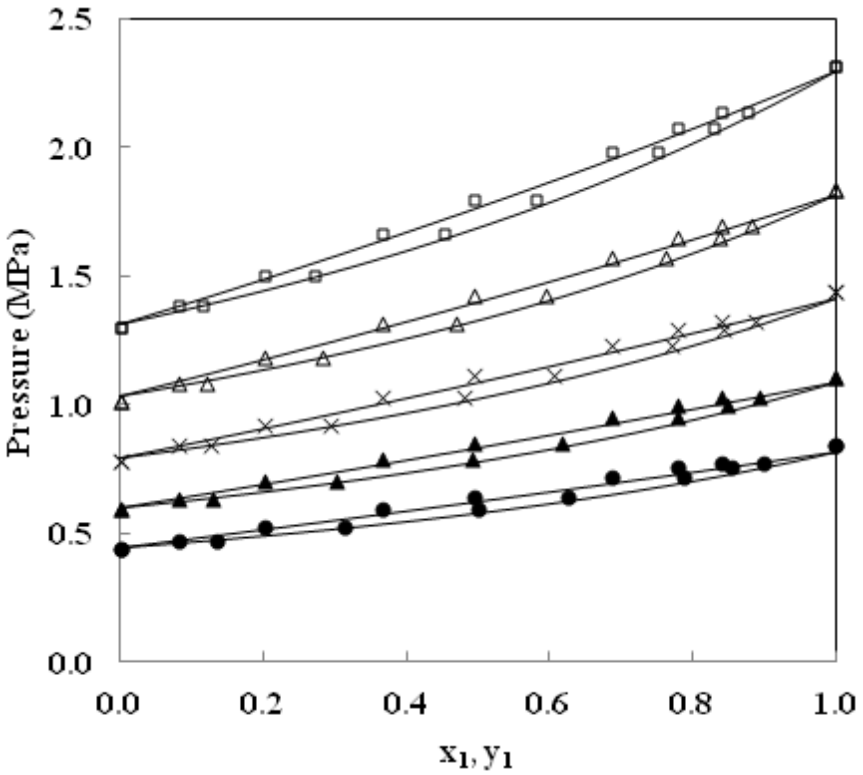

Fig. 33 - VLE prediction for R-143a (1) + R-1234yf (2).
Experimental data [33]**: (●) 283.15 K; (▲) 293.15 K;**
(×) 303.15 K; (∆) 313.15 K; (□) 323.15 K.
NEoS: (——) k_{ij} = 0.

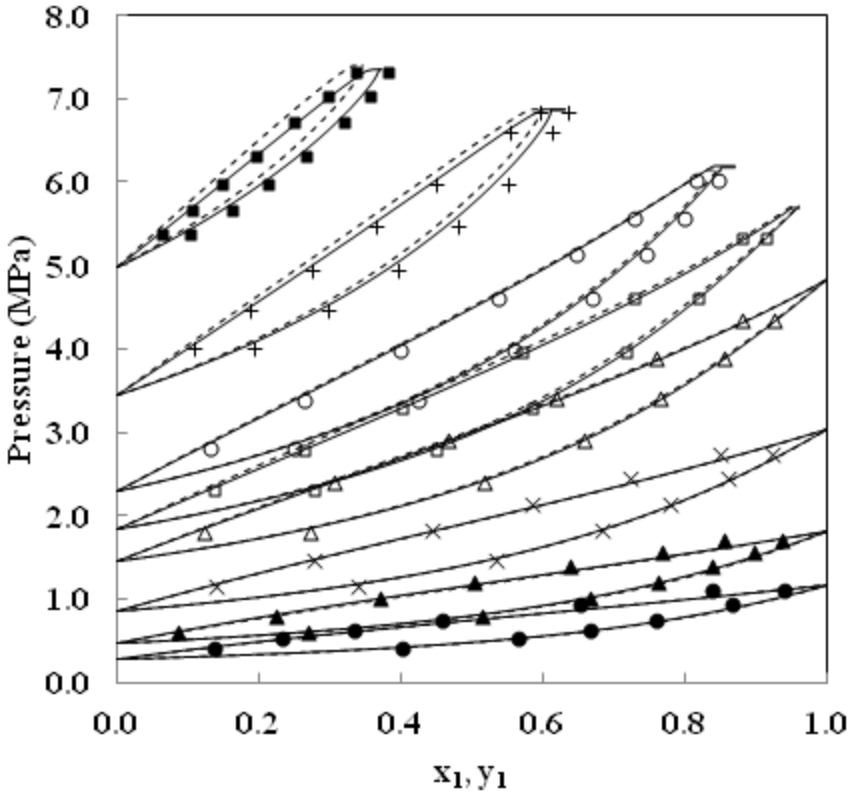

Fig. 34 - VLE prediction for SO_2 (1) + R-32 (2).
Experimental data [34]**: (●) 288.07 K; (▲) 303.16 K;**
(×) 323.15 K; (Δ) 343.15 K; (□) 353.15 K; (○) 363.15 K;
(+) 383.18 K; (■) 403.16 K.
NEoS: (——) k_{ij} = 0; (- - - -) k_{ij} adjusted.

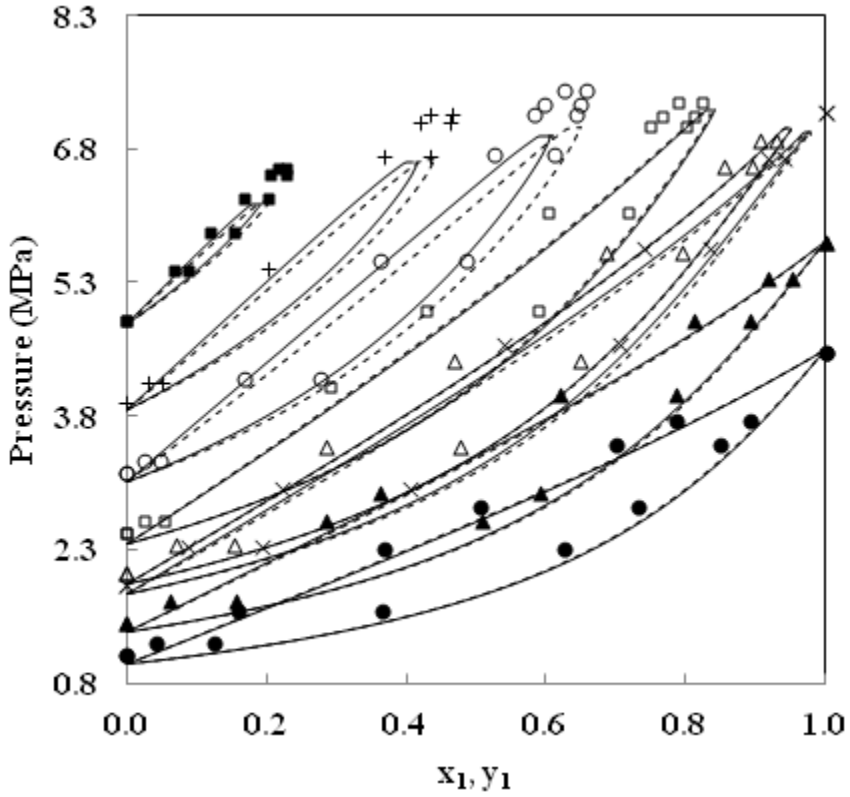

Fig. 35 - VLE prediction for CO_2 (1) + R-32 (2).
Experimental data [35]**: (●) 283.12 K; (▲) 293.11 K;**
(×) 303.13 K; (Δ) 305.15 K; (□) 313.30 K; (○) 323.34 K;
(+) 333.33 K; (■) 343.23 K.
NEoS: (——) k_{ij} = 0; (- - - -) k_{ij} adjusted.

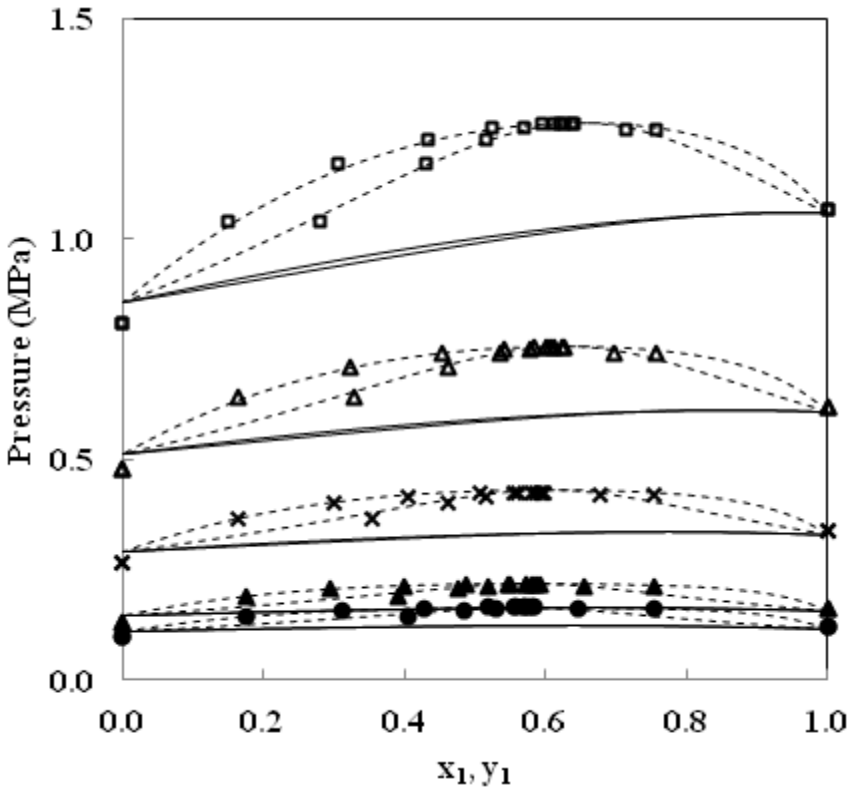

Fig. 36 - VLE prediction for R-23 (1) + R-116 (2).
Experimental data [36]**: (●) 194.33 K;**
(▲) 199.71 K; (×) 214.19 K; (∆) 229.63 K;
(□) 244.94 K.
NEoS: (——) k_{ij} = 0; (- - - -) k_{ij} adjusted.

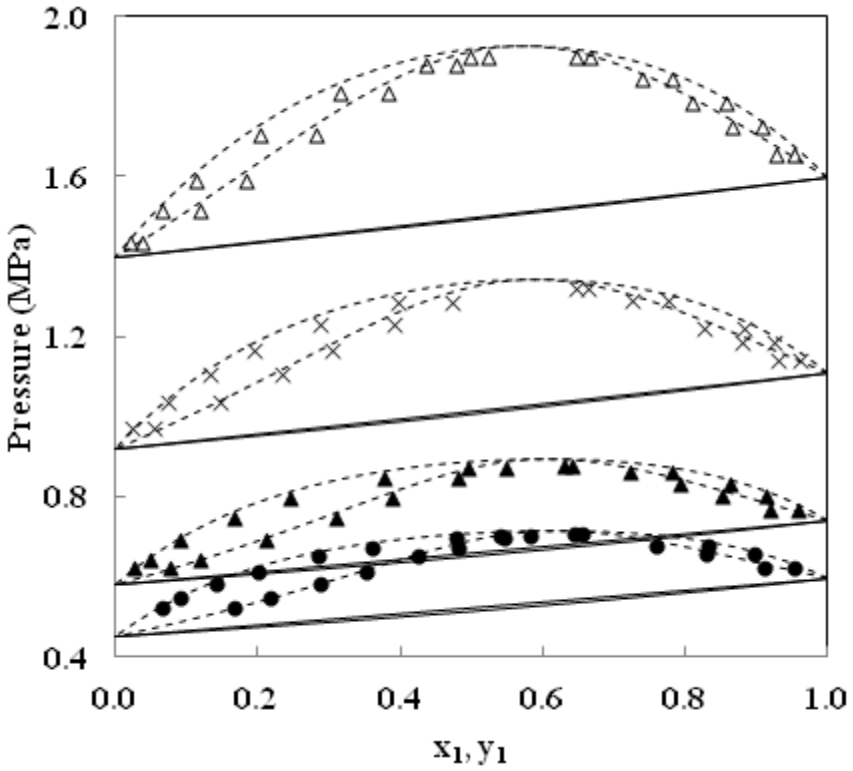

Fig. 37 - VLE prediction for isopentane (1) + R-365mfc (2).
Experimental data [37]**: (●) 363.12 K;**
(▲) 373.20 K; (×) 393.22 K; (Δ) 413.09 K.
NEoS: (——) k_{ij} = 0; (- - - -) k_{ij} adjusted.

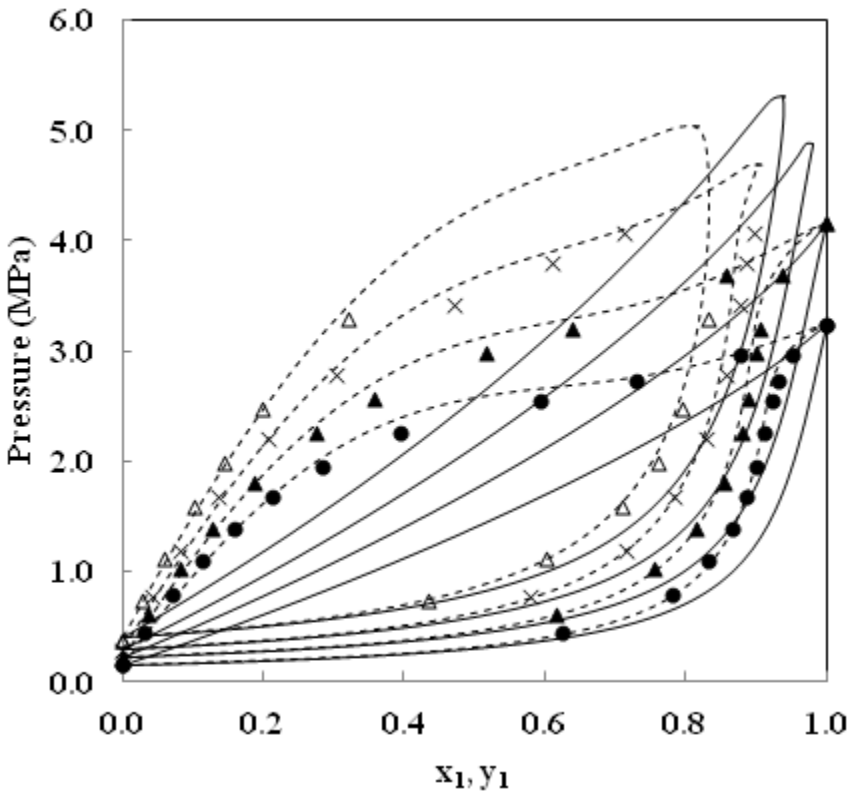

Fig. 38 - VLE prediction for R-23 (1) + butane (2).
Experimental data [38]**: (●) 283.15 K; (▲) 293.15 K;**
(×) 303.15 K; (∆) 313.15 K.
NEoS: (——) k_{ij} = 0; (- - - -) k_{ij} adjusted.

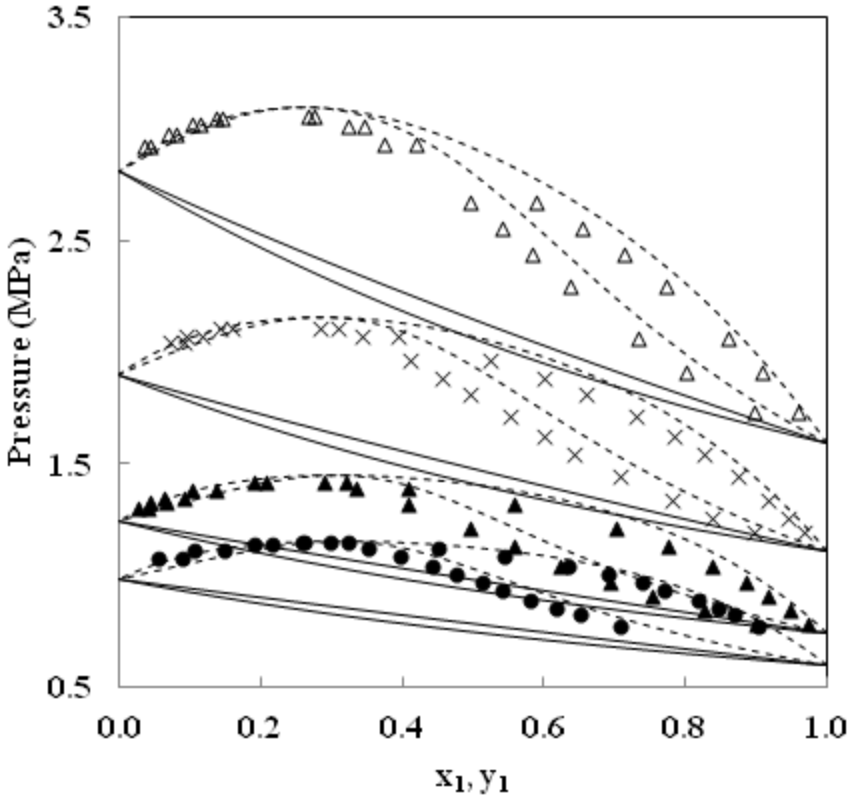

Fig. 39 - VLE prediction for isopentane (1) + R-245fa (2).
Experimental data [37]**: (●) 362.94 K; (▲) 373.17 K;**
(×) 392.87 K; (∆) 412.91 K.
NEoS: (——) k_{ij} = 0; (- - - -) k_{ij} adjusted.

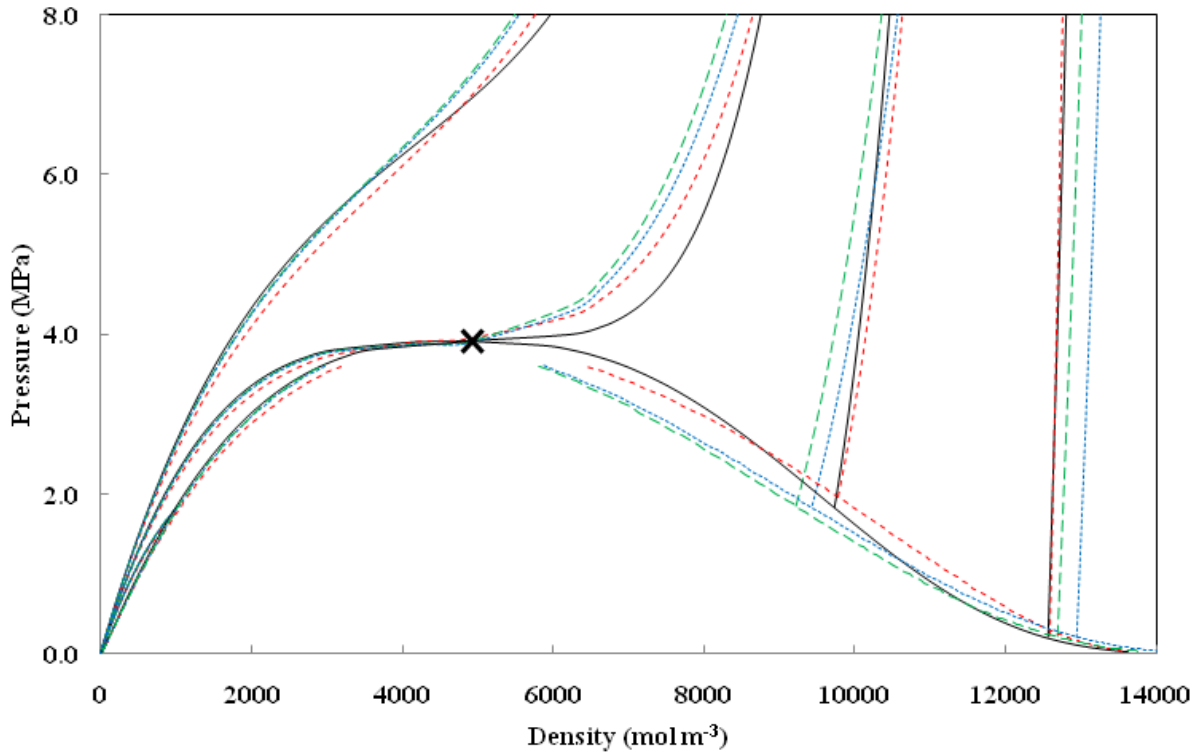

Fig. 40 - P-ρ diagram for R-421A.
(—) REFPROP; (×) Critical Point: REFPROP (T_c = 355.93 K); (- - - -) NEoS; (.....) PT-EoS; (— — —) PR-EoS. Out of saturation: T_r = 0.7, 0.9, 1.0, 1.1.

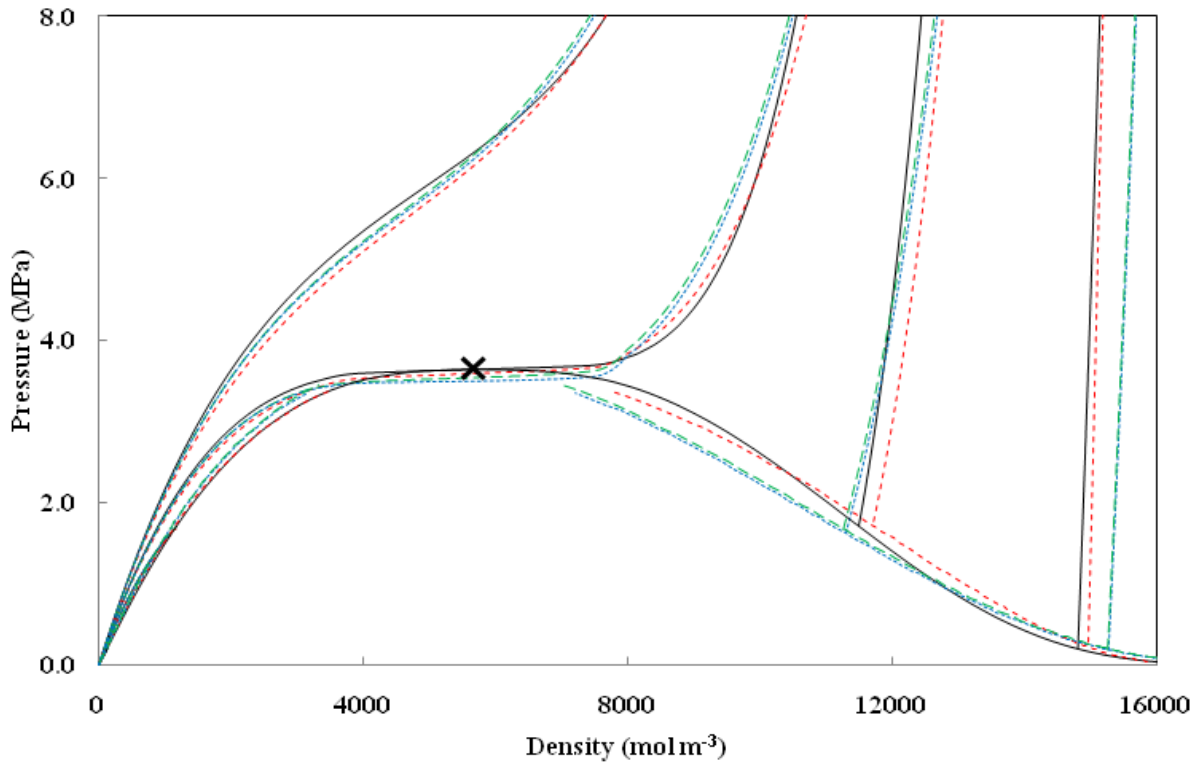

Fig. 41 - P-ρ diagram for R-508A.
(——) REFPROP; (×) Critical Point: REFPROP (T_c = 283.34K); (- - - -) NEoS; (.....) PT-EoS; (— — —) PR-EoS. Out of saturation: T_r = 0.7, 0.9, 1.0, 1.1.

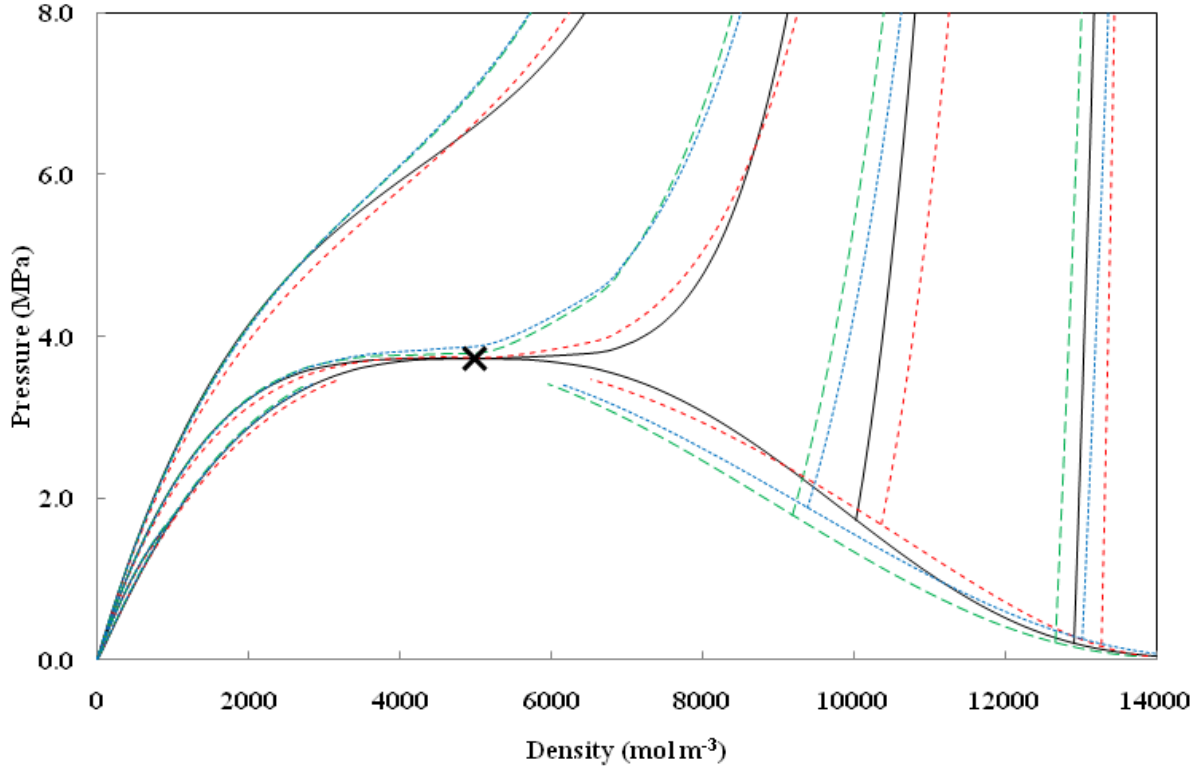

Fig. 42 - P-ρ diagram for R-404A.
(—) REFPROP; (×) Critical Point: REFPROP (T_c=345.2 K); (- - -) NEoS; (.....) PT-EoS; (— — —) PR-EoS. Out of saturation: T_r = 0.7, 0.9, 1.0, 1.1.

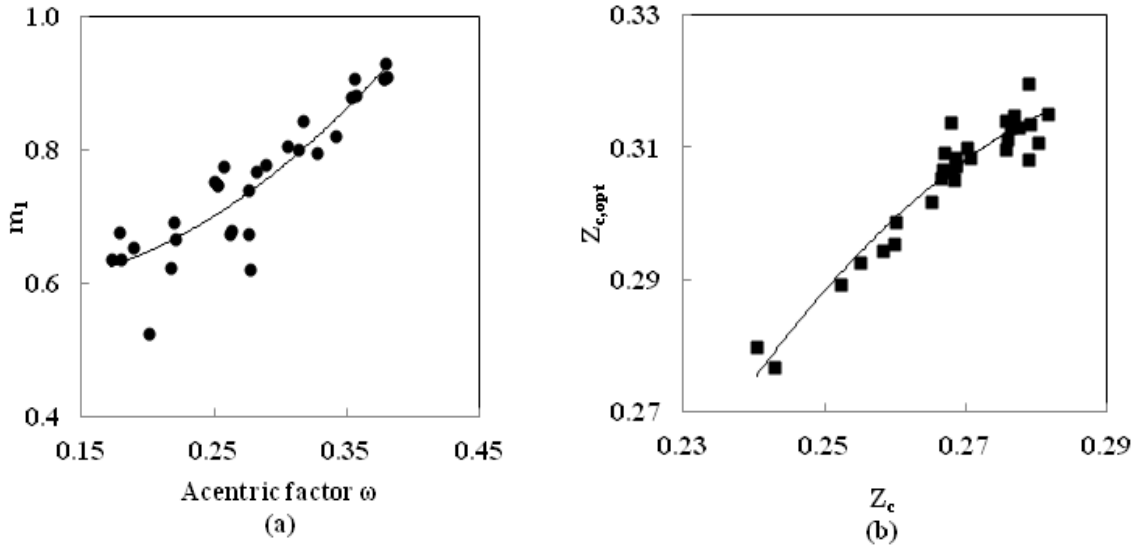

Fig. A.1 - Correlations obtained with the PT-EoS. (a): the m_1 parameter as a function of the acentric factor ω (coefficient of determination $R^2 = 0.83$). (b): the optimized critical compressibility factor $Z_{c,opt}$ as a function of the experimental critical compressibility factor Z_c (coefficient of determination $R^2 = 0.92$).

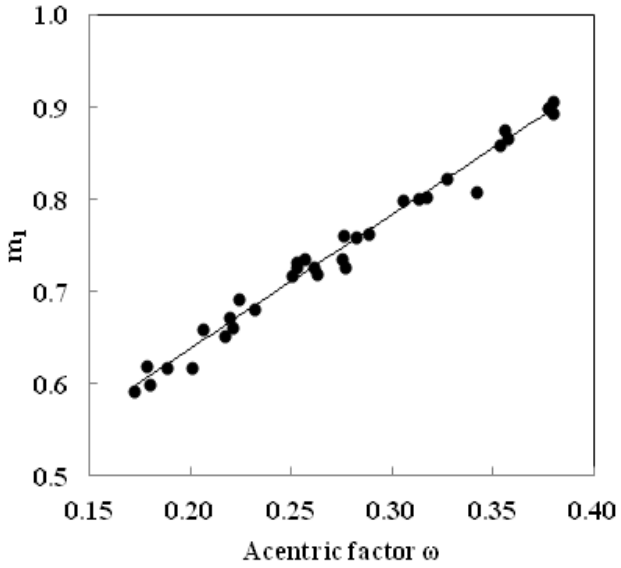

Fig. B.1 - Correlation obtained with the PR-EoS: m_1 parameter as a function of the acentric factor ω (coefficient of determination $R^2 = 0.98$).

SUPPLEMENTARY CONTENT

Prediction of thermodynamic properties of refrigerant fluids with a new three-parameter cubic equation of state

Prédiction des propriétés thermodynamiques des fluides frigorigènes avec une nouvelle équation d'état cubique à trois paramètres

Christophe Coquelet, Jamal El Abbadi, Céline Houriez

Mines ParisTech, PSL Research University, CTP – Centre Thermodynamique des Procédés, 35 rue Saint Honoré, 77305 Fontainebleau Cedex, France

Table A.9 – k_{ij} values used with the NEoS and PR-EoS, for the azeotropic and supercritical systems.

		Binary interaction parameter k_{ij}	
Systems	**T (K)**	**NEoS**	**PR-EoS**
SO_2 + R-32	288.07	0.0030	-0.0189
	303.16	0.0044	-0.0152
	323.15	0.0008	-0.0183
	343.15	-0.0035	-0.0191
	353.15	-0.0067	-0.0205
	363.15	-0.0031	-0.0188
	383.18	-0.0082	-0.0036
	403.16	-0.0165	-0.0133
CO_2 + R-32	283.12	-0.0023	0.0196
	293.11	0.0030	0.0212
	303.13	0.0068	0.0373
	305.15	0.0008	0.0167
	313.30	-0.0028	0.0174
	323.34	0.0189	0.0276
	333.33	0.0119	0.0363
	343.23	0.0129	0.0600
R-23 + R-116	194.33	0.0890	0.1025
	199.71	0.0901	0.1033
	214.90	0.0907	0.1043
	229.63	-	0.1068
	244.94	-	-
Isopentane + R-365mfc	363.12	0.1168	0.1233
	393.22	0.1161	0.1250
	373.20	0.1189	0.1261
	413.09	0.1111	0.1218
R-23 + butane	283.15	0.1915	0.2012
	293.15	0.1904	0.2007
	303.15	0.1885	0.1993
	313.15	0.1905	0.2023

Isopentane + R-245fa	363.12	0.1168	0.1233
	393.22	0.1161	0.1250
	373.20	0.1189	0.1261
	413.09	0.1111	0.1218

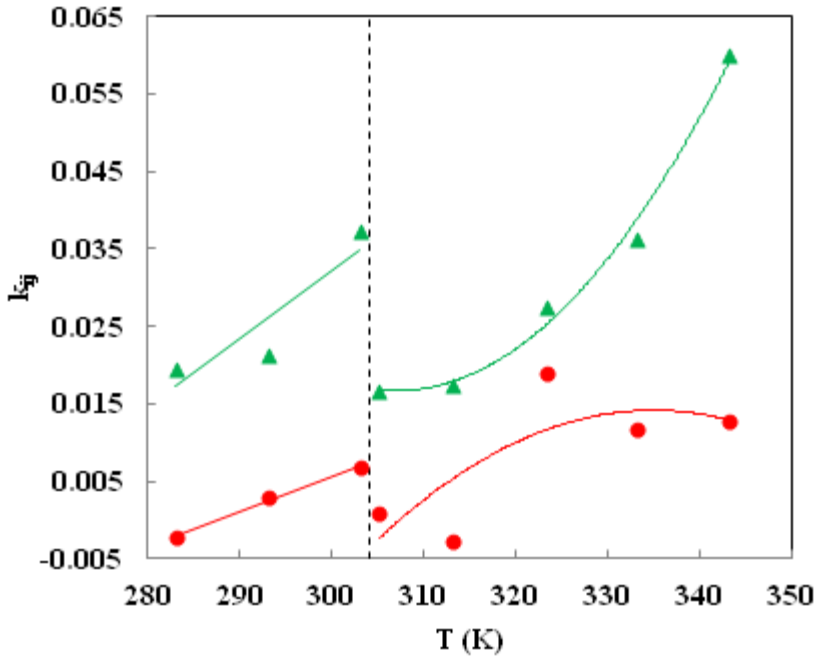

Fig. A.43 - k_{ij} as a function of temperature: CO_2 + R-32.
(●) NEoS; (▲) PR-EoS;
(- - - -) CO_2 critical temperature (T_c = 304.13 K).

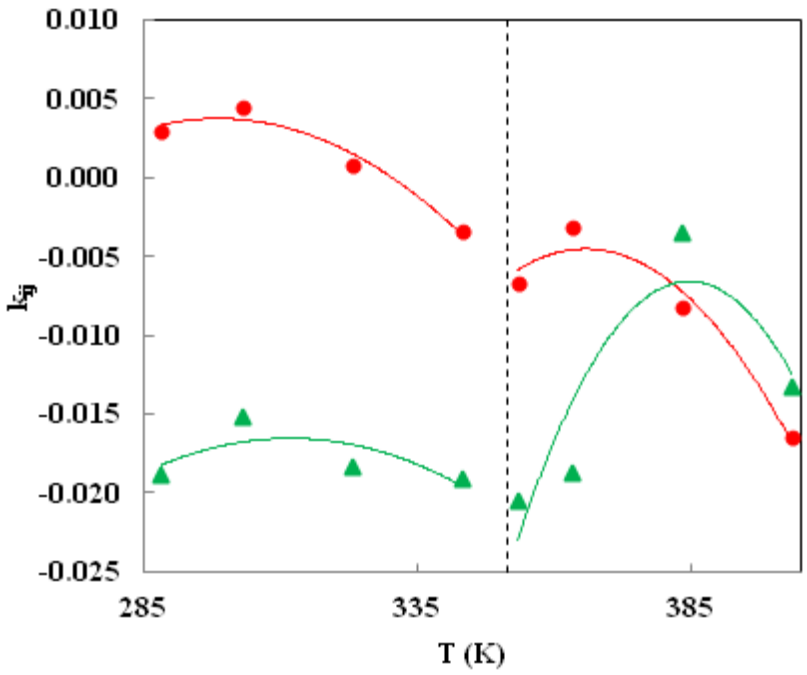

Fig. A.44 – k_{ij} as a function of temperature: SO_2 + R-32.
(●) NEoS; (▲) PR-EoS;
(- - - -) R-32 critical temperature (T_c = 351.26 K).

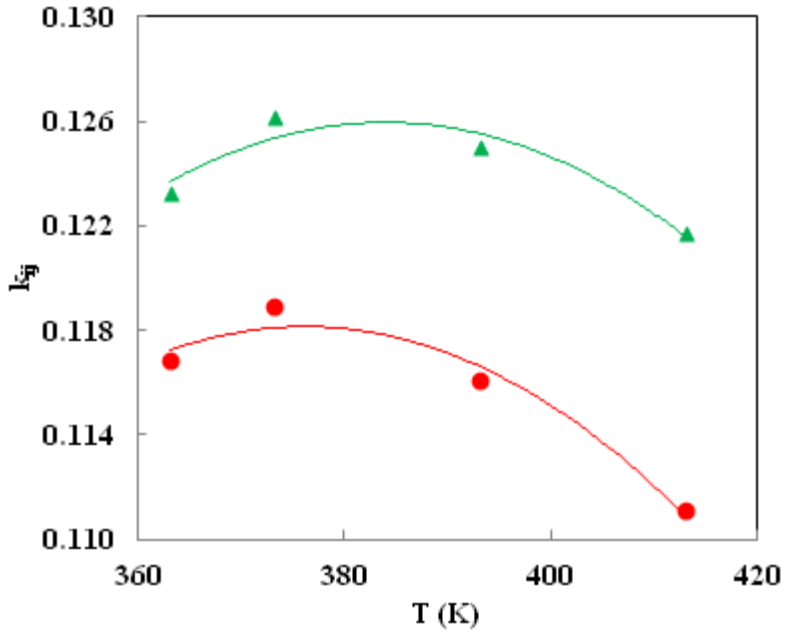

Fig. A.45 - k_{ij} as a function of temperature: isopentane + R-365mfc. (●) NEoS; (▲) PR-EoS.

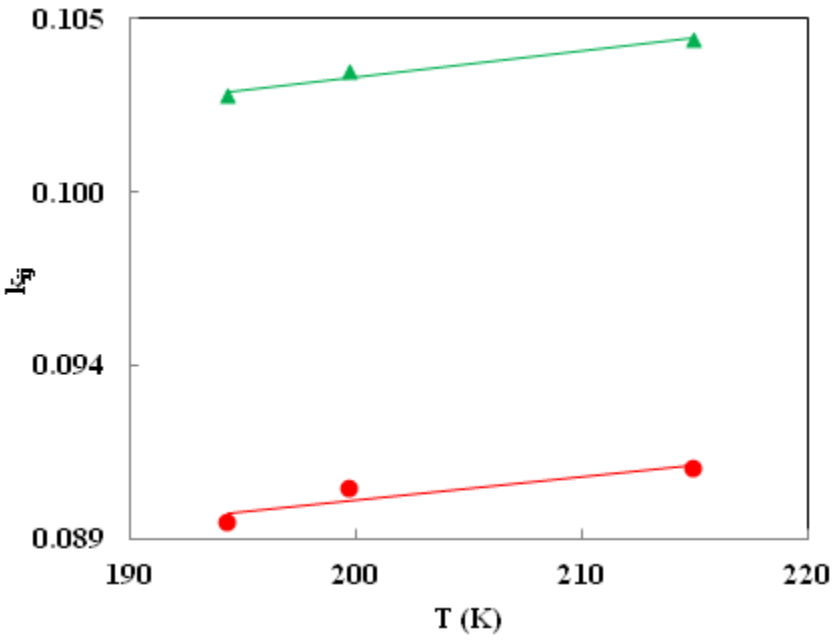

Fig. A.46 - k_{ij} as a function of temperature:
R-23 + R-116.
(●) NEoS; (▲) PR-EoS.

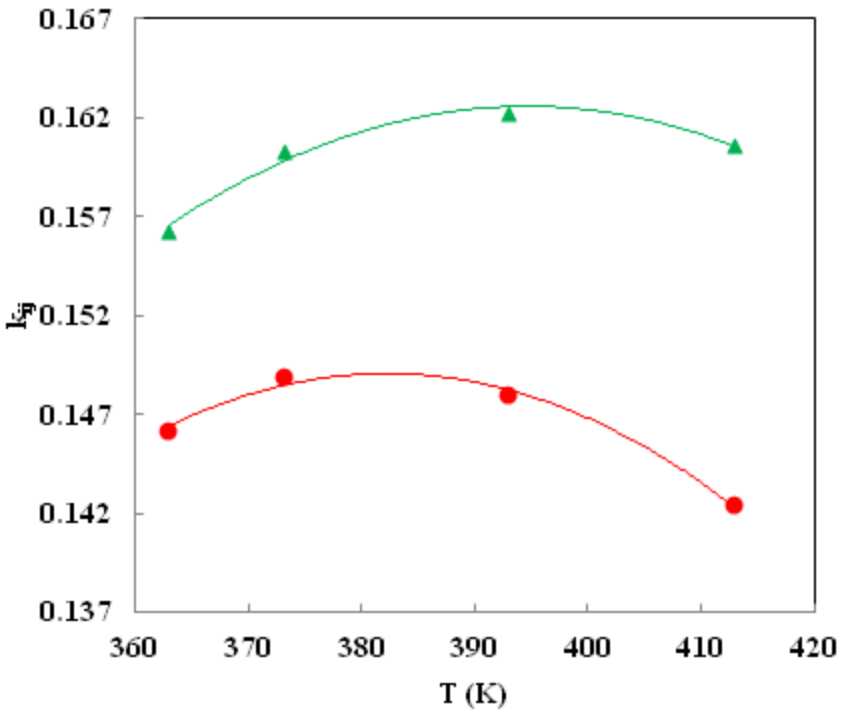

Fig. A.47 - k_{ij} as a function of temperature:
isopentane + R-245fa.
(●) NEoS; (▲) PR-EoS.

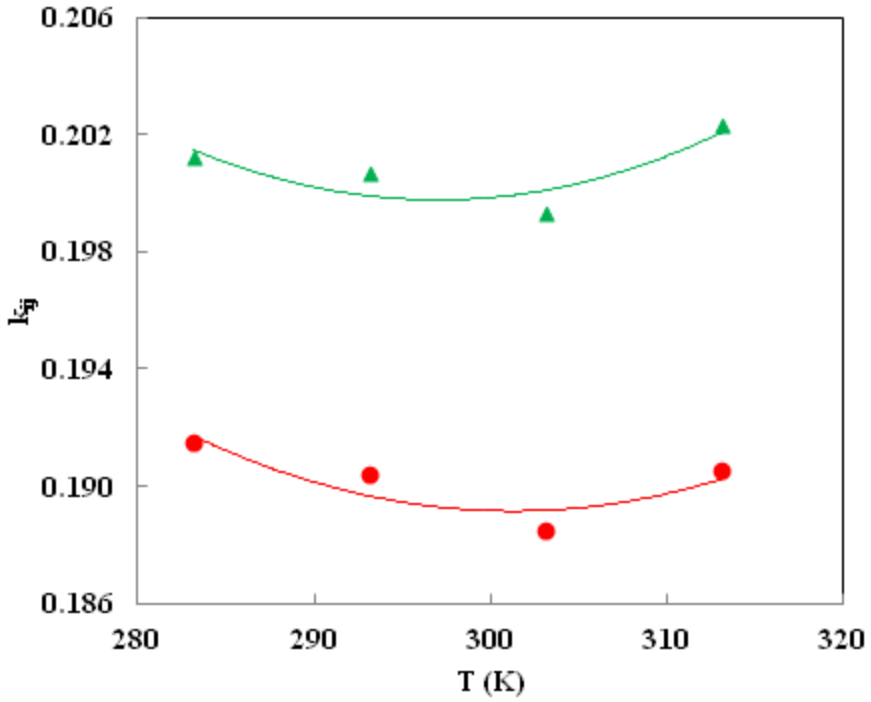

Fig. A.48 - k_{ij} as a function of temperature:
R-23 + butane.
(●) NEoS; (▲) PR-EoS.

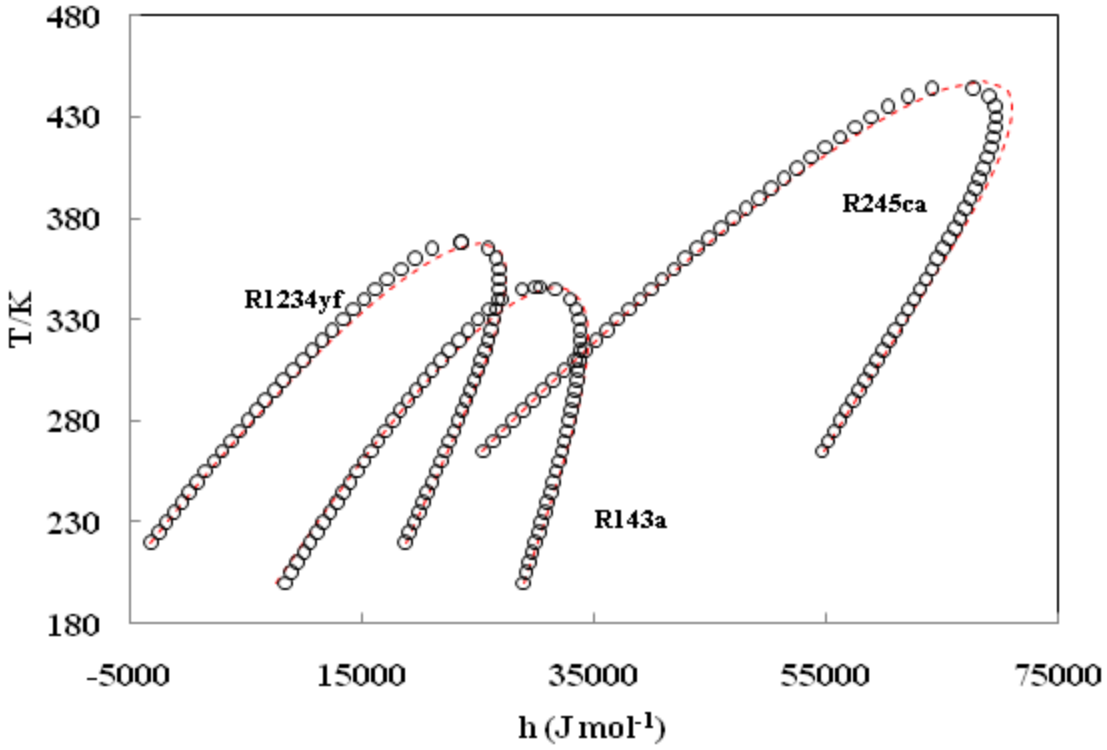

Fig. A.49 – Enthalpies of saturated phases. (○) REFPROP. (- - - -) NEoS.

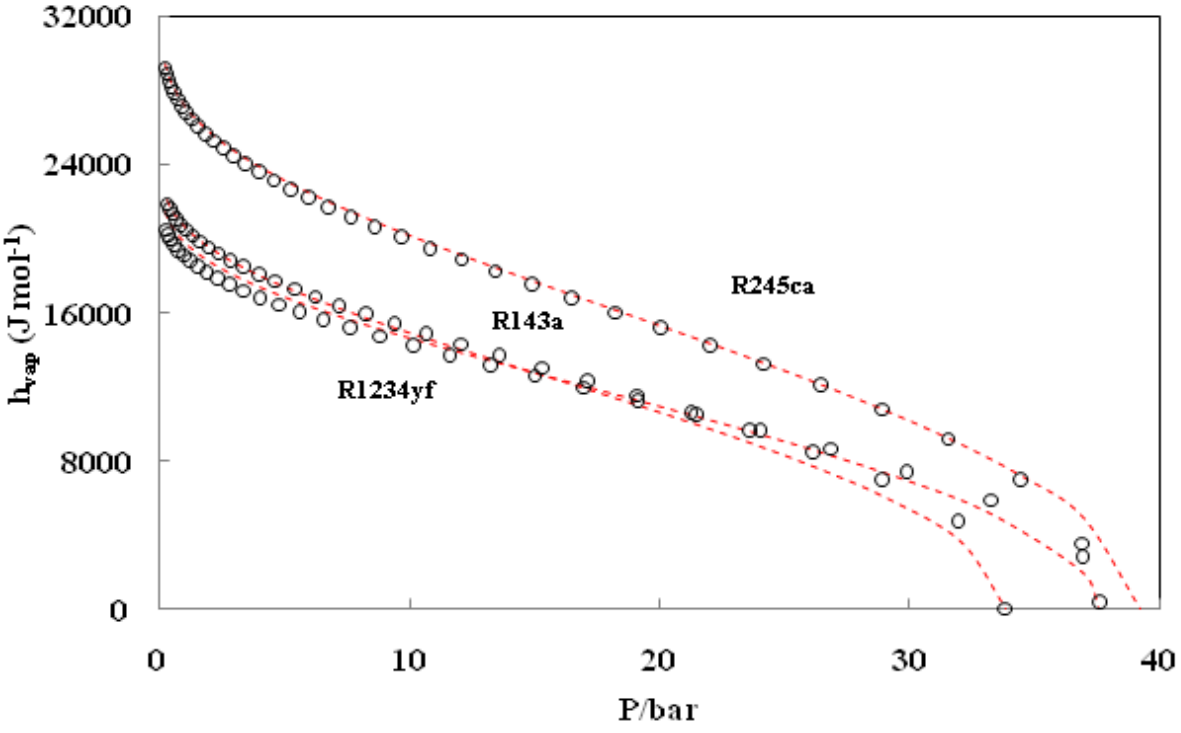

Fig. A.50 – Enthalpies of vaporization. (○) REFPROP; (- - - -) NEoS.

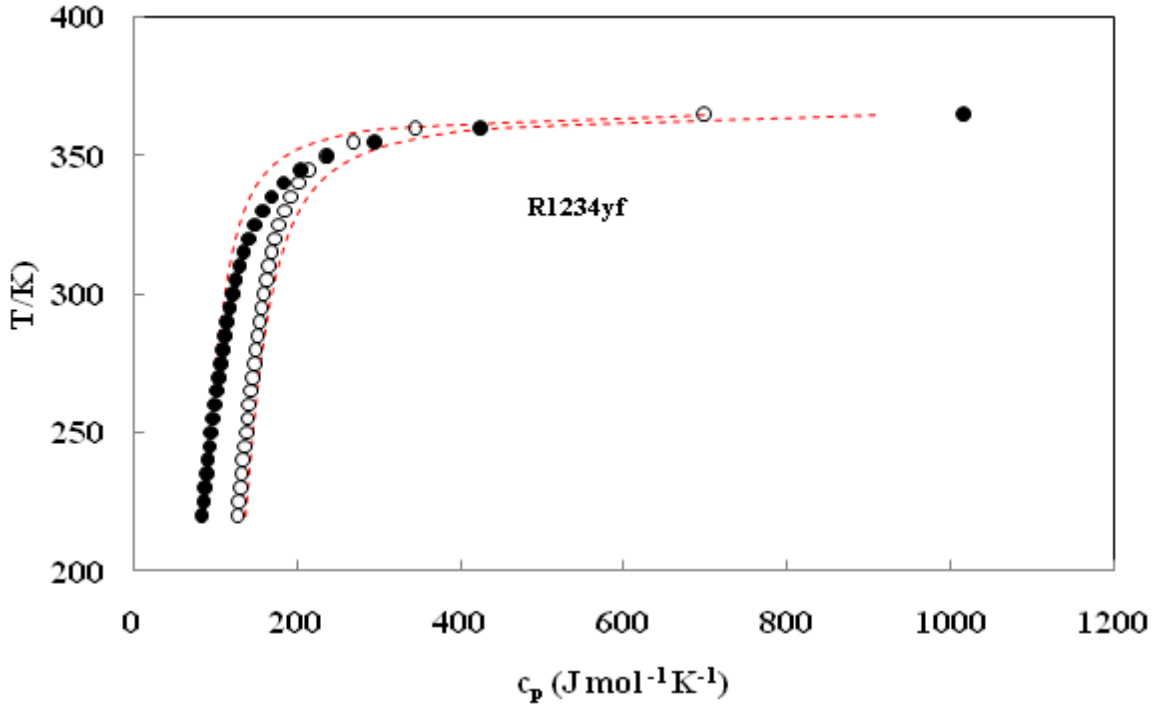

Fig. A.51 – Isobaric heat capacities of saturated phases. (○) Liquid, (●) Vapor – REFPROP; (- - - -) NEoS.

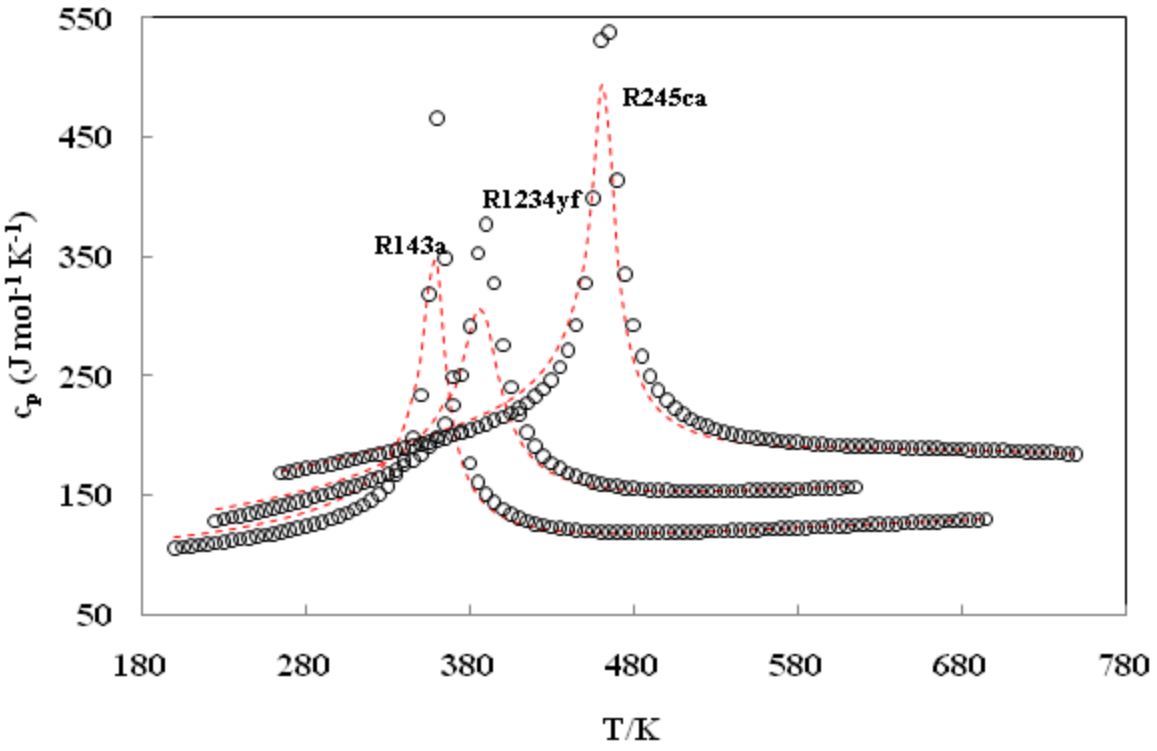

Fig. A.52 – Isobaric heat capacities at P = 5 MPa. (○) REFPROP; (- - -) NEoS.